Received 6 November 2023; revised 11 December 2023; accepted 5 January 2024. Date of publication 15 January 2024; date of current version 1 February 2024.

Digital Object Identifier 10.1109/OJCOMS.2024.3353770

RIS-Assisted Integrated Sensing and Communication Systems: Joint Reflection and Beamforming Design

MOHAMED I. ISMAIL [1], ABDULLAH M. SHAHEEN [2], MOSTAFA M. FOUDA [3] (Senior Member, IEEE), AND AHMED S. ALWAKEEL [2]

[1]Department of Electronic Engineering and Communication Technology, Modern Academy for Engineering and Technology, Cairo 4410242, Egypt
[2]Department of Electrical Engineering, Faculty of Engineering, Suez University, Suez 8151650, Egypt
[3]Department of Electrical and Computer Engineering, College of Science and Engineering, Idaho State University, Pocatello, ID 83209, USA

CORRESPONDING AUTHOR: M. M. FOUDA (e-mail: mfouda@ieee.org)

The work of Mostafa M. Fouda was supported by the National Science Foundation of the USA under Award 2210252.

ABSTRACT The Integrated Sensing and Communication (ISAC) system merged with Reconfigurable Intelligent Surface (RIS) has recently received much attention. This paper proposes an intelligent metaheuristic version of Enhanced Artificial Ecosystem Optimizer (EAEO) for a suggested beamforming optimization framework in ISAC systems with RIS. Two RIS are utilized in the presented model to enhance the received signal-to-noise ratio (SNR) for multiple-input multiple-output (MIMO) communication systems. Also, each element of each RIS scatters the incoming signal with a controllable phase-shift, without increasing its power. The signal is transmitted by a Dual-Function Base Station (DFBS) that is integrated with the RIS, which performs both communication and sensing functions simultaneously. The ISAC system is designed to optimize the signal transmission through the RIS by maximizing the SNR to increase the overall performance. In the proposed EAEO version, a Fitness-Distance-Balance Model (FDBM) is combined with the standard Artificial Ecosystem Optimizer (AEO) to improve the quality of the solutions in multidimensional and nonlinear optimization scenarios. The simulation results show that the proposed EAEO algorithm improves the SNR of different users for different numbers of RIS elements. The SNR reaches 25 dB when using 200 RIS elements. Moreover, the proposed EAEO is tested on the IEEE Congress on Evolutionary Computation 2017 (IEEE CEC'17) test suite. A comparative analysis is conducted compared to the standard AEO and several recent algorithms. The proposed EAEO derives great effectiveness and robustness over the others as it provides a higher rate of success in achieving the global optimum point.

INDEX TERMS Reconfigurable intelligent surfaces, wireless communication, artificial ecosystem optimizer, fitness distance-based model.

I. INTRODUCTION

THE next generation of wireless systems is anticipated to offer extremely fast communication rates and precise sensing services to support cutting-edge applications like automated manufacturing, augmented/virtual reality (AR/VR), smart homes, unmanned aerial vehicle (UAV), and autonomous driving [1], [2]. The concept of ISAC has emerged as a promising technology for wireless systems beyond the generations of 5th-generation cellular network (5G) and sixth-generation cellular networks (6G) [3], aiming to enhance spectral efficiency and reduce hardware expenses [4], [5]. Its implementation seeks to achieve these goals by combining sensing and communication capabilities. Research in integrated sensing and communication primarily focuses on two directions. The first direction investigates dual-functional radar and communication systems [2], where the same hardware is used for both radar and communication functions. By sharing hardware, these systems can achieve

higher spectrum efficiency. However, the dual functions also impose stringent requirements on the hardware in terms of waveforms, architectures, and algorithms. The second research direction [6], [7], examines communication and radar systems that operate separately but utilize the same frequency band. In this case, interference mitigation techniques are important to allow the radar and communication systems to coexist effectively. While the systems remain separate, this approach offers more flexibility in the design of the radar and communication systems.

However, the improvement from using ISAC is limited to the existing Line-of-Sight (LOS) pathway, which is not valid in most environments A promising technology that can improve the wireless propagation environment through adding more pathways is reconfigurable intelligent surfaces [8]. A RIS generally includes a completely passive array of phase shifters that can be remotely adjusted to introduce a specific phase shift to the incoming signal (beamforming) [9]. The beamformers are designed with two objectives for the target directions. First, their goal is to guarantee that every user equipment (UE) attains a minimum necessary signal-to-interference plus noise ratio (SINR). This provides enough signal strength in relation to noise and interference to provide good communication performance for the UEs. Second, the beamformers aim to minimize the radar sensing Cramer-Rao lower bound [2]. The Cramer-Rao lower bound is a measure of the best achievable accuracy for parameter estimation using a given sensing technique. By lowering this bound, the accuracy of radar parameter estimation can be improved, resulting in better sensing performance [10].

We handle two configurations with several users and targets. In the first, we leverage a single RIS to enhance the communication performance of the ISAC system by creating beams that fit a particular beam pattern and guarantee an appropriate SINR for every user. In the second scenario, we assume that users and targets are geographically apart and that only one comm-RIS situated adjacent to the UEs cannot effectively feel the targets, necessitating the adoption of a second RIS, referred to as radar-RIS, for sensing. In this instance, the ISAC system is supported by two customized RISs, and the beams are designed to optimize the worst-case target illumination power while guaranteeing a particular SINR for every user. We show that, despite a small decrease in radar target illumination power, the single-RIS assisted ISAC system under consideration improves the minimal user SINR. Conversely, the dual-RIS assisted ISAC system improves the minimum user SINR as well as the worst-case target illumination power at the targets, especially in situations where the targets and users are not clearly visible. A list of potential research directions on RIS and ISAC is presented in the next subsection.

A. RELATED WORK

The related work is organized as follows: first, describe some of the earliest ISAC research, and then talk about the need for new technologies like RIS that can be used in challenging propagation environments. After that, we exhibit several studies on integrating RIS with ISAC. Finally, check out some research on optimization techniques that address issues with the beamforming optimization framework in integrated sensing and communication systems with RIS.

ISAC systems contain a variety of works. The initial study [11], concentrated on the oversimplified scenario of one communication user and one target. Later, this was expanded to take into account the case of many receivers and large number of sensing targets [2], [12], [13]. As an example, the transmit beamformers were modified by the authors in [3] to reduce multiuser interference for communication users while also attaining the necessary transmit beampattern for sensing applications. In their early investigation, the standard radar waveform was used by the authors [14], [15] as a carrier for sensing and data transmission. In addition, the mmWave frequency spectrum is appealing to ISAC systems due to its wide bandwidth, which enables higher data speeds and more accurate placement [16]. The pathloss, which can be so severe that non-line-of-sight (NLoS) communications are frequently too weak to be of any practical use, makes it challenging to operate at mmWave frequencies, which restricts reliable communication or sensing. Moreover, the previously methods [10], [17] cannot provide the required levels of radar or communication performance if the direct links to the UEs or targets are inefficient or nonexistent.

Reconfigurable intelligent surfaces, an emerging technology with many passive elements, are attracting a lot of focus with regarding wireless communications [8], [18], localization [19], and radar sensing [20], [21]. With a controller, usually located at the base station, a two-dimensional array of phase shifters, called RIS, can be independently controlled. Although RISs are not capable of performing data acquisition, channel estimation, or symbol decoding, they can be designed to introduce virtual LoS paths and favorably alter the wireless propagation environment [22], [23]. This allows communication or sensing even in situations where the direct path is weak or blocked.

Recently, numerous works have proposed incorporating RIS into ISAC to increase SINR and target illumination power, particularly when the direct channel from the BS to the UEs or targets is blocked [21], [24], [25], [26]. Transmit beamformers, sometimes called waveforms, and RIS phase shifts are typically engineered to achieve desired communication and sensing performance levels. The majority of the works consider relatively simple scenarios, like using only one antenna for communications [27], or single user multiple targets [28], multiple users single target [29], [30]. In their most generic form, [21], [31], [32], [33] discusses the settings of RIS-assisted ISAC systems for multiple users and targets. In [21], information is communicated and sensed via a single dedicated transmit waveform. For an ISAC system with independent colocated subarrays for sensing and communication, the transmit beamformers and reflection coefficients are constructed in [31]. The signal received at the

RIS will also take up a lot of radar waveforms because radar and communication subarrays are so close to one another. This will increase interference at the UEs but is ignored in [31]. Furthermore, target detection is impossible anytime the direct pathways to the targets are blocked because the DFBS senses the targets directly without any help from the RIS.

A practical method for reducing mutual interference in wireless communication systems is to deploy RIS next to a communication device, as was done in the development of the dual-functional RIS-aided ISAC system [21]. When there is no direct path between the dual-functional radar and communication (DFRC) BS and the sensing target, the study mentioned in [25] uses RIS to achieve joint localization and communication. An algorithm for RIS passive beamforming as well as a target localization technique were recommended by the authors. In a more general scenario where the DFRC BS and target are in close contact, the authors of [26] suggested a revolutionary method that makes use of a single RIS for both sensing and communication needs. The coexistence of MIMO radar and multi-user communication systems in the shared spectrum presents an interference management challenge, as explored by [24] using RIS. The joint trajectory, sensing, and communication design of UAV were taken into consideration in [34]. Using RIS, the coexistence of multi-user communication systems and MIMO radar in the common spectrum was investigated in [24].

A radar-communication-coexistence (RCC) system with RIS assistance is considered in [32]. For sensing and communication, this system makes use of transceivers that are not dependent on geography. The goal of the study in [32] is limited to the radar system's communication interference minimization; radar waveform design to attain a specific radar performance is not considered. The total radar SNR owing to multiple targets is the radar performance statistic that is used to build independent communication and sensor beamformers, according to [33]. One target may receive all of the power if the total radar SNR is utilized as a radar metric, which could result in one or more targets being completely missed by the radar system.

In addition, [21], [31], [32], [33] think about a situation where the RIS isn't being used for radar sensing. Therefore, it is not viable to build extra routes that provide reliable sensing if the targets are not immediately accessible to the DFBS using the benefit of RIS [20]. The RIS is usually used at higher frequencies.High-speed transmission and high-accuracy perception are strengths of Terahertz (THz) and millimeter wave communications, but they require a narrow beamwidth to compensate for a significant route loss. In order to enable beam switching, the authors [35] propose a system-level beam alignment method that makes use of the synchronization signal block (SSB) supplied for beam management and SSB-based sensing. In [36], the strategies needed to effectively implement and oversee next-generation THz wireless networks—which will work together to facilitate a fellowship of communication and sensing services—are examined from every viewpoint. To improve THz wireless networks-based extended reality (XR) experiences, [37] presents a novel joint sensing, communication, and artificial intelligence (AI) framework. They proposed a system that yields comprehensive historical sensing data and predictive predictions of upcoming environmental changes that may be applied to variations in known and expected user behaviors as well as environmental conditions. This permits passive radar (PR) to occupy the space.

Passive radar, which uses radar data to pinpoint a target without using its own controlled emissions, has undergone extensive research over the past 80 years [38], [39]. Authors in [40] emphasise that enhanced localization and sensing by PR are predicted to be made possible in large part by RIS. Due to their cheap cost of acquisition, use, and maintenance as well as its capacity for covert operation, passive radar deployment has a number of distinct advantages [41]. Locating targets with limited information is essential in PR. In fact, the passive radar is protocol independent, in contrast to conventional radar. In other words, the PR is unaware of the transmit waveform information. However, due to a lack of assistance from active components, PR can occasionally fail to carry out target localization. Overall, the new technique looks like it will be helpful for many different radar applications.The authors of [42] examine the application of RIS for radar detection in situations when there isn't a direct relationship between the radar and the target. This is critical in a range of real-world civilian and military situations. In fact, the so-called "around-the-corner radar" is a contemporary and very challenging challenge for security concerns, particularly in urban environments where small moving targets, such as humans and small UAV, are widely present [43], [44], [45], [46]. Such targets usually fall in a shadow region (produced by a tall structure, for example) that blocks the LOS. Therefore, new approaches are required to adjust signal and data processing to this unique propagation environment in order to control the problem. The primary strategies developed in the public domain rely on natural multipath capitalization or radar networks. Beamforming optimization framework is necessary to realize the benefit of supporting the RIS in the ISAC system. To resolve this problem, a variety of optimization strategies can be applied.

One of these optimization algorithms is the AEO algorithm which is recently developed by W. Zhao et al. [47]. AEO requires just small alterations in engineering domains and is easily adaptable. With the intention of achieving the highest value for fitness, the AEO strategy integrates three energy transfer processes, consumption, and decomposition—into an ecosystem. Nevertheless, throughout the AEO approach's consumption process, the search space is investigated to find new candidate solutions, and the already-existing solutions are utilized to raise their fitness ratings. Numerous real-world engineering optimisation issues have been addressed using the AEO technique. These include choosing the best

electrical representation for PV cells [48], planning the path of unmanned combat aerial vehicles (UCAVs) [49], modelling groundwater levels [50], solving the economic dispatch problem with combined heat and power (CHP) units [51], optimizing the allocation of distributed generation and capacitors in power networks [52], and estimating energy costs [53]. This paper introduces an EAEO as a framework for optimizing beamforming in reconfigurable intelligent surfaces integrated with sensing and communication systems.

The basic AEO is integrated with the FDBM in the proposed EAEO version to improve the quality of the solutions in multidimensional and nonlinear optimization settings. For the optimal power flow problem, it has been effectively used [54]. Based on the Euclidean distance metric, the FDBM enables operations for intensification and diversity. The combined FDBM choosing technique makes it possible to consistently and successfully select members of a population who would be most beneficial to the search operations. The proposed EAEO is evaluated using a test suite for the IEEE CEC'17, which consists of 28 different numerical benchmark functions. The EAEO approach is found to deliver optimal performance when compared to the original AEO [47] and several recent metaheuristic algorithms including the slime mould algorithm (SMA) [55], enhanced SMA (ESMA) [56], [57], and using the olden search optimizer (GSO) [58], and circle optimizer (CO) [59] in order to adjust the cascaded PD-PI controller. The main contribution of the paper is summarized in the next subsection.

B. MAIN CONTRIBUTION

The main contributions made in this work are as follows:

1) The Fitness Distance Balance model with Artificial Ecosystem Optimization (FDBAEO), has been developed to achieve improved performance.
2) An EAEO integrating FDBM is developed to handle beamforming optimization framework in integrated sensing and communication systems with RIS.
3) The proposed EAEO technique is validated on the CEC'17 test suite demonstrating great superiority over AEO, SMA, ESMA, GSO, and CO.
4) Furthermore, the proposed EAEO declares higher resilience and stability than the others.
5) Multiple users and targets are handled by two configurations, which are suitable for different situations:
    a) We construct beams with strong cross-correlation features to fit a desired beam pattern and guarantee an acceptable SINR for each user, all in an effort to improve the communication performance of the ISAC system using a single RIS.
    b) There are two RISs specifically used, and the beams are engineered to optimize the worst-case target illumination power while ensuring a specific SINR for every user.
6) Numerical simulations demonstrate the advantages of the proposed approach for RIS-assisted ISAC systems.

In the paper, the performance improvement, of joining RIS and ISAC, is studied in different scenarios. In the first scenario, the RIS is used for communication enhancement only. In the second scenario, a dual-RIS assisted ISAC system is used for both communication and radar improvement. The first setting is suitable for aerial surveillance or in conditions with little scattering when the targets are directly visible to the DFBS via a direct path. On the other hand, the second setting is suitable for situations when the direct path to the targets is barred or very weak, such as the localization of cars or pedestrians in an urban context, that is, for settings with rich scattering. The advantage of using the proposed EAEO algorithm in RIS-assisted ISAC systems is illustrated through simulation. Moreover, the simulation results show that the SNR has been improved and reached 25 dB when increasing the number of RIS elements to 200. Furthermore, the EAEO algorithm outperforms other algorithms (e.g., AEO, SMA, ESMA, CO, and GSO).

The benefit of the suggested design for RIS-assisted ISAC systems are shown through numerical simulations. When compared to ISAC without RIS [17], the comm-RIS assisted ISAC system significantly raises the fairness SINR of the communication UEs while only slightly degrading the worst-case target illumination power. The amount of total power transmitted to the comm-RIS that was lost is what causes this loss. Due to the increased degrees of freedom provided by the radar-RIS in the design of the dual-RIS assisted setup with dedicated RISs for sensing and communications, both the fairness SINR and worst-case target illumination power are significantly increased when compared to an ISAC system without RIS [17], especially when all of the targets are not immediately visible to the DFBS.

The remaining sections are structured as follows. In Section II, the system model is described. The design issues and the performance measurements are described in Section III. In Section IV, the suggested solvers are developed. In Section V, numerical simulations showing how well the suggested algorithms work are presented. In Section VI, the paper is concluded.

*Notation:*In this paper, we adopt the following notation: lowercase letters correspond to scalars, while boldface lowercase (uppercase) letters denote vectors (matrices). The operations of transpose, complex conjugation, and Hermitian (i.e., complex conjugate transpose) are represented by $(.)^T$, $(.)^\star$, and $(.)^H$, respectively. We can use $x[n]$ or x_n to denote the n^{th} entry of the vector x. Let $\Omega^N = a \in \mathbb{C}^N : |a_i| = 1, i = 1, \ldots, N$ be the vectors of N-dimension with unit modulus entries, and S_M^+ represents a set of $M \times M$ positive semidefinite matrices.

II. SYSTEM MODEL

In order to enable communication with K individual users who each own a single antenna, a DFRC communication system is considered as part of a MIMO ISAC system with RIS support. Furthermore, by utilizing RIS in the distant field, the system can simultaneously emit radar waves in the

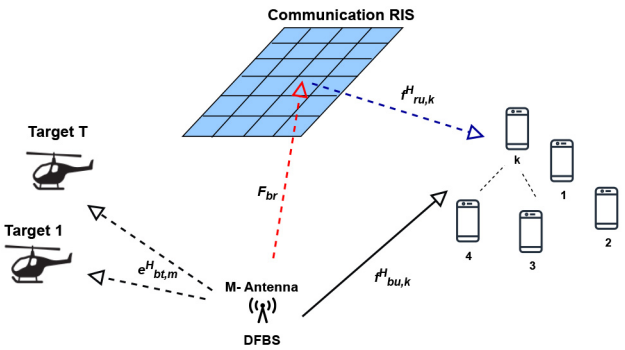

FIGURE 1. Only communication functions are supported by RIS.

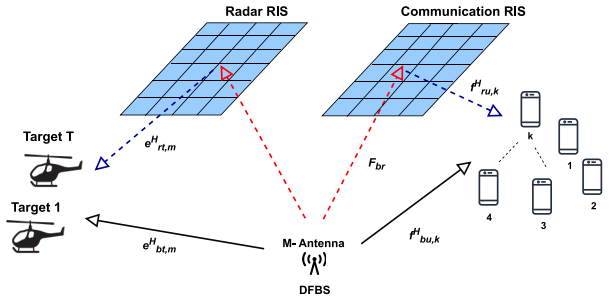

FIGURE 2. Dual RISs for communication and sensing.

direction of T point targets. The DFBS's uniform linear array (ULA), with M antennas, transmits both radar waveforms and communication symbols.

In the system under consideration, it is presumable that the targets and users are spatially well-separated, with the radar-RIS and comm-RIS being closer to the targets and the user equipment respectively. This spatial separation is depicted in Figure 1 and Figure 2. Consequently, wireless connections between the comm-RIS (radar-RIS) and the targets (UEs) are severely attenuated, and their corresponding wireless channel responses can be disregarded without any significant impact on the overall system performance. Due to the fact that the BS transmits two signals, one for radar detecting and the other for data transmission, two appropriate beamformers must be constructed. The optimization challenge is made considerably more difficult to handle by the coupling between the data transmission beamformer and the beamformer for radar sensing. Further consideration is given to the two beamformers in order to lessen radar signal interference. Multiple characteristics, including the number of antennas, are relevant to the radar sensing MSE in the shared scheme [60], [61].

There are two different scenarios for joining RIS with ISAC. The first scenario is applicable when the targets are in direct line of sight to the DFBS via a clear path, for example, during aerial monitoring or under low scattering conditions. Conversely, the second scenario is more appropriate for situations where the targets' direct path is blocked or greatly attenuated, such as in urban environments where vehicles or pedestrians need to be localized. In such settings, the scattering of signals is typically rich and can be exploited to achieve effective target localization.

1) *First Scenario (Figure 1):* In the system under consideration, a comm-RIS placed near the UEs, is used to improve the performance of the system by enhancing communication. The RIS phase shifts and the transmit beamformers are jointly optimized to ensure uncorrelated beams and minimize the received SINR at the UEs. However, this optimization problem is non-convex.[1] To overcome this challenge, the transmit beamformers are designed with fixed RIS phase shifts, and vice versa, to iteratively optimize both the beamformers and phase shifts. The comm-RIS phase shifts are optimized based on the beamformers to maximize SINR.

2) *Second Scenario (Figure 2):* An ISAC system assisted by two dedicated RISs is suggested. A single comm-RIS, situated close to UEs, is unable to effectively sense the targets, this led to the employment of a second RIS known as radar-RIS for sensing. Because both RISs are passive, uncorrelated beams can't be created for radar sensing, as happened before. As a result, we make sure that the UEs obtain a minimum SINR while maximizing the worst-case target illumination power. For designing the phase shifts of the radar-RIS, a method based on semi-definite relaxation followed by Gaussian randomization is suggested. Meanwhile, the same process used in the first setup is employed for designing the phase shifts of the comm-RIS. The system model incorporates various channel models, which will be elaborated upon in subsequent subsections.

A. DOWNLINK TRANSMIT SIGNAL MODEL

The downlink transmit signal model is defined as follows: $\boldsymbol{x}_n = [x_1[n], \ldots, x_M[n]]^T \in \mathbb{C}^{M\times 1}$ is used to identify the discrete-time baseband radar waveforms at a certain moment n, while $\boldsymbol{y}_n = [y_1[n], \ldots, y_K[n]]^T \in \mathbb{C}^{K\times 1}$ represents the complex baseband downlink communication symbols sent to the K UEs in discrete time. Using the communication beamformer $\boldsymbol{P} = [\boldsymbol{p}_1, \boldsymbol{p}_2, \ldots, \boldsymbol{p}_K] \in C^{M\times K}$, the $\boldsymbol{y}_n$ is precoded, and with the sensing beamformer $\boldsymbol{Q} = [\boldsymbol{q}_1, \boldsymbol{q}_2, \ldots, \boldsymbol{q}_M] \in C^{M\times M}$, the $\boldsymbol{x}_n$ is precoded. The DFBS transmits the precoded radar waveforms and communication symbols overlaid. The DFBS transmits a complex baseband signal that is

$$\boldsymbol{z}_n = \boldsymbol{P}\boldsymbol{y}_n + \boldsymbol{Q}\boldsymbol{x}_n \in C^{M\times 1} \tag{1}$$

1. Due to the quadratic equality, the optimization problem is non convex. The non-convexity is specifically caused by the fractional SINR expression in constraints and the closely related optimization variables. Furthermore, because the objective function and constraints have continuous channel state information (CSI) uncertainty sets, the optimization issue under consideration is a semi-infinite programming problem with an infinite number of constraints. The SINR constraint, which encompasses the interference term, has an unlimited number of restrictions due to CSI error [62]). As a result, it is typically intractable for the construction of a reliable resource allocation algorithm. Moreover, the SINR-constrained beampattern matching has become the standard ISAC design criterion. This typically results in quadratic semidefinite programming (QSDPs), which raises the computational complexity of determining the best solution overall.

The communication symbols sent to various UEs are presumed to be uncorrelated because the UEs do not collaborate among themselves. Also, assume the radar and communication symbols have unit power and are not correlated ($\boldsymbol{R}_d = E[\boldsymbol{y}_n \boldsymbol{y}_n^H] = I_M$, $\boldsymbol{R}_w = E[\boldsymbol{x}_n \boldsymbol{x}_n^H] = I_M$ and $E[\boldsymbol{y}_n \boldsymbol{x}_n^H] = 0$). Thus, the transmit signal covariance matrix $\boldsymbol{R} = E[z_n z_n^H] \in S_M^+$ which is determined by

$$\begin{aligned}\boldsymbol{R} &= E\Big[\big(\boldsymbol{P}\boldsymbol{y}_n + \boldsymbol{Q}\boldsymbol{x}_n\big)\big(\boldsymbol{P}\boldsymbol{y}_n + \boldsymbol{Q}\boldsymbol{x}_n\big)^H\Big] \\ &= E\Big[\big(\boldsymbol{P}\boldsymbol{y}_n + \boldsymbol{Q}\boldsymbol{x}_n\big)\big(\boldsymbol{y}_n^H\boldsymbol{P}^H + \boldsymbol{x}_n^H\boldsymbol{Q}^H\big)\Big] \\ &= \boldsymbol{P}\boldsymbol{P}^H + \boldsymbol{Q}\boldsymbol{Q}^H \\ &= \sum_{k=1}^{K} \boldsymbol{p}_k \boldsymbol{p}_k^H + \boldsymbol{Q}\boldsymbol{Q}^H = \sum_{k=1}^{K} \boldsymbol{P}_k + \boldsymbol{Q}\boldsymbol{Q}^H \end{aligned} \tag{2}$$

where the rank-1 matrix $\boldsymbol{P}_k$ was first introduced as $\boldsymbol{P}_k = \boldsymbol{p}_k \boldsymbol{p}_k^H$.

B. RIS MODEL

A low-rate control link from the DFBS can be used to independently control each separate passive shifters[2] phase shifter that makes up the RIS. Specifically, the spatial response of the RIS is modeled as that of Uniform Rectangular Arrays (URAs) comprising N elements. The phase shifts of the RIS are collected in the vector $\boldsymbol{s}_t = [s_{t,1}, s_{t,2}, ..s_{t,N}] \in \Omega^{1\times N}$, where $s_{t,i}$ signifies the phase shift produced by the i^{th} RIS element, and $t \in (u, v)$ with u and v stand for the comm-RIS and radar-RIS, respectively.In the first scenario, the RIS just enhances the ISAC's communication capabilities; in this case, the broadcast signal travels through the RIS both directly and indirectly to reach the UEs, but only directly to the target. In the second scenario, there is a dual-RIS configuration with a sensor and a communications-focused RIS. In the second scenario, users (targets) additionally receive signals via the comm-RIS (the radar-RIS) in addition to the direct channel, which is used by both users and targets.

C. COMMUNICATION CHANNEL MODEL

Consider a multi-user MIMO scenario in which K single antenna UEs are in communication with the DFBS. Let $\boldsymbol{F}_{br} \in C^{N\times M}$ stand for the DFBS-comm-RIS link's MIMO channel matrix. Let $\boldsymbol{f}_{bu} \in \mathbb{C}^{1\times M}$ and $\boldsymbol{f}_{ru} \in \mathbb{C}^{1\times N}$ indicate the vectors of the multiple-input single-output (MISO) channels associated with the k^{th} UE for the DFBS-UE and RIS-UE links, respectively. The complete channel vector $\boldsymbol{f}_k^H$, containing both the direct link and the additional link made possible by the RIS, is expressed as follows:

$$\boldsymbol{f}_k^H = \boldsymbol{f}_{bk,k} + \boldsymbol{f}_{ru,k} diag(\boldsymbol{s}_u) \boldsymbol{F}_{br} \in C^{1\times M} \tag{3}$$

where $diag(\boldsymbol{s}_u)$ is the phase shift of comm-RIS. The signal received at k^{th} UE at time n is given by

$$r_k[n] = \boldsymbol{f}_k^H \boldsymbol{z}_n + n_k[n] = \boldsymbol{f}_k^H \big[\boldsymbol{P}\boldsymbol{y}_n + \boldsymbol{Q}\boldsymbol{x}_n\big] + n_k[n] \tag{4}$$

where $n_k[n]$ represents the additive receiver noise, known as additive white Gaussian noise (AWGN), which follows a Gaussian distribution with a mean of zero and a variance of σ^2.

D. RADAR CHANNEL MODEL

Let ϕ_j to denote the angular position of the j^{th} target with respect to the directional fixed beamforming system. The channel between the DFBS and the j^{th} target is represented by a LOS channel and is expressed as follows:

$$\boldsymbol{e}_{bt,j}^H = \alpha_{bt,j} \boldsymbol{a}^H\big(\phi_j\big) \in C^{1\times M} \tag{5}$$

In the above equation, $\alpha_{bt,j}$ denotes the complex path gain, and $\boldsymbol{a}(.)$ represents the DFBS array response vector. The path leading to the j^{th} target from the radar-RIS is represented by the vector $\boldsymbol{e}_{rt,j}^H \in \mathbb{C}^{1\times N}$. The channel that results between the DFBS and the jth target is obtained as follows:

$$\boldsymbol{e}_j^H = \boldsymbol{e}_{bt,j}^H + \boldsymbol{e}_{rt,j}^H diag(\boldsymbol{s}_v) \boldsymbol{E}_{br} \in C^{1\times M} \tag{6}$$

Here, $\boldsymbol{E}_{br} \in \mathbb{C}^{N\times M}$ denotes the channel between DFBS and the radar-RIS. Let $\boldsymbol{s}_v$ to be zero whenever the radar-RIS is not being used or made unavailable.

III. PROBLEM FORMULATION

In this paper, we present a methodology for designing transmit beamformers and RIS reflection patterns that improve the performance of the ISAC system. The proposed approach leverages various communication and radar sensing metrics to optimize performance under specific system constraints. The resulting beamformers at the DFBS and RIS phase shifts for two different system configurations are evaluated to illustrate the efficacy of the proposed approach.

A. COMMUNICATION METRICS

The spectral efficiency of the UEs is considered the performance parameter in a multi-user MIMO communication system's quality of service. This spectral efficiency can be determined using the SINR at each user. The worst-case SINR is used, also known as the "fairness SINR", as the communication metric to guarantee a minimum SINR for each UE.

Let's express the signal that was received at the k^{th} UE, or (4), as an expression for the SINR as

$$r_k[n] = \boldsymbol{f}_k^H \left[\boldsymbol{p}_k \boldsymbol{y}_k[n] + \sum_{j=1, j\neq k}^{K} \boldsymbol{p}_j \boldsymbol{y}_j[n] + \sum_{m=1}^{M} \boldsymbol{q}_m \boldsymbol{x}_m[n]\right] + n_k[n] \tag{7}$$

2. Note that, RISs that are active, as opposed to passive, have phase and reflection-type amplifiers that are capable of amplifying incident signals [22], [23]. In contrast to systems that use decode-and-forward relays or fully active sensors in place of passive phase shifters, active RISs are devoid of radio frequency (RF) chains [63]. When compared to conventional passive RISs for communications, active RISs perform noticeably better [22], [23]. However, when building systems with active RISs, active amplifier components should be taken into consideration because they provide extra noise, also known as RIS noise, to the system.

where the received signal at the k^{th} UE is made up of three components: the desired communication symbol, the interference resulting from communication symbols intended for other UEs, and the interference caused by radar waveforms. As a result, the SINR for the k^{th} UE is a function of $\boldsymbol{s}_u, \boldsymbol{P}, \boldsymbol{Q}$ and is given by

$$\begin{aligned}\gamma_k(\boldsymbol{s}_u, \boldsymbol{P}, \boldsymbol{Q}) &= \frac{|\boldsymbol{f}_k^H \boldsymbol{p}_k|^2}{\sum_{j=1, j\neq k}^{K} |\boldsymbol{f}_k^H \boldsymbol{p}_j|^2 + \sum_{m=1}^{M} |\boldsymbol{f}_k^H \boldsymbol{q}_m|^2 + \sigma^2} \\ &= \frac{\boldsymbol{f}_k^H \boldsymbol{p}_k \boldsymbol{p}_k^H \boldsymbol{f}_k}{\boldsymbol{f}_k^H \left(\sum_{j=1, j\neq k}^{K} |\boldsymbol{p}_j \boldsymbol{p}_j^H + \boldsymbol{Q}\boldsymbol{Q}^H|\right) \boldsymbol{f}_k + \sigma^2} \\ &= \frac{\boldsymbol{f}_k^H \boldsymbol{P}_k \boldsymbol{f}_k}{\boldsymbol{f}_k^H (\boldsymbol{R} - \boldsymbol{P}_k) \boldsymbol{f}_k + \sigma^2} \end{aligned} \tag{8}$$

with the worst case SINR

$$\gamma_{min} = \min_k \gamma_k(\boldsymbol{s}_u, \boldsymbol{P}, \boldsymbol{Q}) \tag{9}$$

B. RADAR SENSING METRICS

The effectiveness of sensing can be measured in two situations: *1)* When employing radar-RIS; and *2)* When do not employ radar-RIS. These two situations bring two objective functions in the radar sensing metrics: *1)* The average squared cross-correlation of the reflected signals and beampattern mismatch error; and *2)* The worst-case target illumination power. These objective functions are discussed in more detail below.

1) BEAMPATTERN MATCHING AND CROSS-CORRELATION ERROR

Targets are located and tracked by a MIMO radar system that transmits signals in predetermined directions. To do this, many beams with distinct beam patterns are created, with the association between them kept to a minimum [2], [64]. A desirable pattern $d(\phi)$ must be selected that has major beams pointing in various target directions in order to guarantee sufficient power reaches various target places. Additionally, the comm-RIS is only effective if enough power actually reaches it. Hence, the required pattern should likewise create a beam from the DFBS in the comm-RIS direction, indicated by ζ_r.As a result, the required pattern is therefore found to be a superposition of numerous rectangular beams with centers at about $(\phi_k)_{k=1}^{T}$ and ζ_r as

$$d(\phi) = \begin{cases} 1 & \text{if } \phi \in [\phi_k - \epsilon, \phi_k + \epsilon] \\ 1 & \text{if } \phi \in [\zeta_r - \epsilon, \zeta_r + \epsilon] \\ 0 & \text{otherwise} \end{cases} \tag{10}$$

The DFBS emits power in the direction of ϕ in the form of

$$J(\phi) = E\left[|\boldsymbol{a}^H(\phi)\boldsymbol{z}_n|^2\right] = \boldsymbol{a}^H(\phi)\boldsymbol{R}\boldsymbol{a}(\phi) \tag{11}$$

The beampattern mismatch error is calculated for a desired beampattern $d(\phi)$ across a discrete grid of L angles $(\hat{\phi}_i)_{i=1}^{L}$ as a function of R given by

$$L_1(R, \tau) = \frac{1}{L} \sum_{l=1}^{L} |J(\overline{\phi}_l) - \tau d(\overline{\phi}_l)|^2 \tag{12}$$

where τ is the unidentified auto-scale parameter. When the targets are pointed in directions i and j, the cross-correlation of the reflected signals is given by

$$\begin{aligned} J_c(R, \overline{\phi}_i; \overline{\phi}_j) &= E\left[\boldsymbol{r}^*[n; \phi_i] \ \boldsymbol{r}[n; \phi_j]\right] \\ &= E\left[\boldsymbol{a}^H(\overline{\phi}_i) z_n z_n^H \boldsymbol{a}(\overline{\phi}_j)\right] \\ &= \boldsymbol{a}^H(\overline{\phi}_i) \boldsymbol{R} \boldsymbol{a}(\overline{\phi}_j) \end{aligned} \tag{13}$$

such that $\boldsymbol{r}[n; \phi] = \boldsymbol{a}^H(\phi)\boldsymbol{z}[n]$. Average squared cross-correlation data show

$$L_2(R) = \frac{2}{T^2 - T} \sum_{i=1}^{T-1} \sum_{j=i+1}^{T} |J_c(R, \overline{\phi}_i; \overline{\phi}_j)|^2 \tag{14}$$

where $\frac{T^2-T}{2}$ is a pairs of a distinct directions in the set ϕ_i normalized. Radar beams are designed with the goal of minimizing the average squared cross-correlation and the weighted total beampattern mismatch error [64].

$$L(R, \tau) = w_a L_1(R, \tau) + w_b L_2(R) \tag{15}$$

where the weights w_a and w_b, which demonstrate the proportional significance of the two variables, are unknown.

2) WORST-CASE TARGET ILLUMINATION POWER

The target illumination power will be very low if many beams are created at the DFBS towards different targets using the beampattern mismatch criterion when the direct routes between the DFBS and the targets are poor or blocked. Thus, radar-RIS can be utilized to facilitate sensing in these circumstances. Nonetheless, it is impossible to achieve optimum cross-correlation beams directed toward the targets as the RIS has a completely passive nature. In order to construct the sensing beamformers, different measurements are utilized to maximize the worst-case target illumination power.

According to the sent waveform z_n, the signal's power at the m^{th} target is $E[|\boldsymbol{e}_m^H \boldsymbol{z}_n|^2]$. The worst-case target illumination power is provided by

$$\begin{aligned} T(\boldsymbol{R}, \boldsymbol{s}_v) &= \min_m E\left[|\boldsymbol{e}_m^H \boldsymbol{z}_n|^2\right] \\ &= \min_m \boldsymbol{e}_m^H \boldsymbol{z}_n \boldsymbol{z}_n^H \boldsymbol{e}_m \\ &= \min_m \boldsymbol{e}_m \boldsymbol{R} \boldsymbol{e}_m \\ &= \min_m Tr(\boldsymbol{R} D_m) \end{aligned} \tag{16}$$

where, $D_m = \boldsymbol{e}_m \boldsymbol{e}_m^H$ and T depends on $\boldsymbol{s}_v$ through $\boldsymbol{e}_m$(*c.f.* Eq. (6)), $m = 1, .., M$.

C. DESIGN PROBLEMS

This section deals with the challenge of developing the two system designs, transmit beamformers at the DFBS and the RIS phase shifts. We begin by configuring the transmit beamformers $(\boldsymbol{P}, \boldsymbol{Q})$ and comm-RIS phase shifts $\boldsymbol{s}_u$ for the first scenario, as shown in Figure 1. The comm-RIS helps DFBS to communicate with numerous users while maintaining a minimal SINR for all users and minimizing the sensing cost function $L(\boldsymbol{R}, \tau)$ [c.f. Eq. (15)]. Second, the transmit beamformers $(\boldsymbol{P}, \boldsymbol{Q})$, the radar-RIS phase shifts $\boldsymbol{s}_v$ and comm-RIS phase shifts $\boldsymbol{s}_u$ are configured for the second scenario (c.f. Figure 2). To increase the goal illumination power in the worst-case scenario $T(\boldsymbol{R}, \boldsymbol{s}_v)$ [c.f. Eq. (16)], these designed parameters are applied, while providing a minimal SINR for each user. In the first scenario, the design challenge is formulated mathematically as

1^{st} setting

$$\underset{Q,S,\tau,s_u}{minimize} \quad L(\boldsymbol{R}, \tau) \tag{17}$$

(P1) subject to

$$\boldsymbol{R} = \boldsymbol{p}\boldsymbol{p}^H + \boldsymbol{Q}\boldsymbol{Q}^H \in S_{\dagger}^{M} \tag{18a}$$

$$[\boldsymbol{R}]_{i,i} = \frac{Q_t}{M}, i = 1, .., M \tag{18b}$$

$$\gamma_k(\boldsymbol{s}_u, \boldsymbol{P}, \boldsymbol{Q}) \geq \Gamma, k = 1, \ldots, K \tag{18c}$$

$$\boldsymbol{s}_u \in \Omega^N \tag{18d}$$

where, Q_t stands for the maximum allowable transmit power, while (18b) denotes the power constraints per antenna element. Additionally, τ is the auto-scale parameter, and Γ represents the SINR requirement for each user. In the second scenario, the design problem can be expressed as follows:

2^{nd} setting

$$\underset{P,Q,s_u,s_v}{maximize} \quad T(\boldsymbol{R}, s_v) \tag{19}$$

(P2) subject to

$$\boldsymbol{R} = \boldsymbol{p}\boldsymbol{p}^H + \boldsymbol{Q}\boldsymbol{Q}^H \in S_{\dagger}^{M} \tag{20a}$$

$$[\boldsymbol{R}]_{i,i} = \frac{Q_t}{M}, i = 1, \ldots, M \tag{20b}$$

$$\gamma_k(\boldsymbol{s}_u, \boldsymbol{P}, \boldsymbol{Q}) \geq \Gamma, k = 1, \ldots, K \tag{20c}$$

$$\boldsymbol{s}_v \in \Omega^N, \boldsymbol{s}_u \in \Omega^N \tag{20d}$$

As the RIS is entirely passive and reflects the incident signal by adjusting its phase shift in multiple directions, the constraints (18d) and (20d) are enforced. Due to the unit modulus requirement in (18d), the equality in quadratics in (18a), and the fractional term in (18c), the optimization problem (**P1**) is not convex.

A different goal function is employed in (**P2**) as opposed to (**P1**). Moreover, the radar-RIS phase shifts are developed furthermore to the transmit beamformers and comm-RIS phase shifts in (**P2**), the issue with optimization is further complicated by the equality in quadratics (20a), the constraint's fractional term (20c), and the limits on unit-modulus (20d). Consequently, the problem (**P2**) is also non-convex.

IV. PROPOSED EAEO TECHNIQUE

The RIS phase shifter and transmit beamformer designs problems (**P1** and **P2**) are not convex in the variables. And, deterministic algorithms typically struggle to handle NP-hard problems (17,19), as their computing costs are frequently intolerable. Consequently, population-based heuristic algorithms have attracted a lot of interest. Among them, the AEO algorithm outperforms other metaheuristic algorithms such as the SMA [55], ESMA [56], the GSO [58] and CO, in some complex problems due to its many advantages including ease of implementation, simplicity of structure, and powerful search capability. Another effective optimization algorithm is the semidefinite relaxation (SDR), which is an effective approximation method in terms of computation. However, for some practical applications, it has been demonstrated that utilizing semidefinite relaxation-based approximation techniques can significantly increase the likelihood of discovering the global solution of the issue [65], [66], [67]. In the suggested version of EAEO, the traditional AEO is integrated with the FDBM to improve the quality of the solutions in multidimensional and nonlinear optimization scenarios. The EAEO integrating FDBM is created to manage the beamforming optimization framework in integrated sensing and communication systems with RIS.

A. AEO: STANDARD VERSION

Artificial ecosystem-based optimization is a population-based optimizer that is motivated by the energy flow in an ecosystem on Earth. This algorithm imitates the three distinctive behaviours of real creatures, including production, consumption, and decomposition. While the search space exploration can be enhanced as shown in the consumption mechanism and exploitation can be carried out in the decomposition, the production operator in the production mechanism allows AEO to produce a new individual at random. Overall comparisons indicate that AEO exceeds its other cutting-edge competitors in terms of optimization performance. AEO is more competitive than other documented approaches, especially for real-world engineering problems, in terms of convergence rate and computational effort. AEO has an edge in solving tough issues with an uncharted search space [47]. The basic components of AEO are consumption, production, and decomposition, forming the three transference mechanisms of energy in an ecosystem. The primary technique is production, in which this operation allows AEO to produce an individual randomly. The newly added individual is able to select between the best person (AR_{Best}) and an arbitrarily selected person (AR_R) in the area of search to replace the old one. Consequently, the algebraic formulation of the production operation can be represented as follows [47]:

$$AR_1(1 + Ti) = AR_{Best}(Ti) \times \left[1 - Rm_1 \times \left(1 - \frac{Ti}{Ti_{max}}\right)\right] + Rm_1 \times AR_R \times \left(1 - \frac{Ti}{Ti_{max}}\right) \tag{21}$$

$$AR_R = Rm \times (Up - Lp) + Lp \tag{22}$$

where Ti and Ti_{max} are, respectively, the existing iteration and the maximum amount of iterations, Up denotes the higher limit, Lp denotes the lower limit, and Rm_1 denotes an arbitrary vector with an interval of [0, 1]. Additionally, the terms $(Rm(Up-Lp)+Lp)$ and the term $((1-Ti/Ti_{max})Rm_1)$ show, accordingly, a linear weighting factor and the location of a person in the search area.

For an effective exploration of the searching area, Levy flight has been included in the consumption process. This operation replicates the food hunt of a variety of animals since it might be treated as a computational formulation. Levy flying is an example of an effective walk-in randomness that can reach the global optimum despite certain phases taking a very long time to complete while moving slowly. Nevertheless, there seem to exist dual accompanied negatives: the intricacy and the need to adjust a wide range of parameters. In order to enhance the features of the Levy movement, the consumption component has been established as indicated in Eq. (23), which is a parameter-free random.

$$C = 0.5 \times \frac{v_1}{|v_2|}, \quad v_1 \approx v_2 \approx N(0, 1) \tag{23}$$

where the normal distribution $N(0, 1)$ has a mean of (0) and a standard deviation of (1).

Three consumption strategies are made possible by the consumption component. The first strategy, as shown in Eq. (24), is the herbivore, in which the consumer can devour the producer.

$$AR_k(1 + Ti) = AR_k(Ti) + C \times (AR_k(Ti) - AR_1(Ti)), \quad k \in [2{:}P_M] \tag{24}$$

where P_M denotes the number of individuals in the population. The second strategy, carnivore, is represented in Eq. (25), and it allows only consumers with advanced levels of energy to arbitrarily consume consumers.

$$AR_k(1 + Ti) = AR_k(Ti) + C \times (AR_k(Ti) - AR_1(Ti)), \quad k \in [3{:}P_M] \tag{25}$$

The third strategy, referred to as omnivore in Eq. (26), allows consumers to eat producers and consumers at random while still maintaining a high amount of energy.

$$\begin{aligned} AR_k(1 + Ti) = {} & AR_k(Ti) \\ & + C \times (z_2 \times AR_k(Ti) - AR_1(Ti)) \\ & + (1 - z_2)[AR_i(Ti) - AR_k(Ti)], \\ & i = [3{:}P_M], k = r([2i - 1]) \end{aligned} \tag{26}$$

Decomposition represents the third tactic as shown in Eq. (27) which permits each person to bypass the decomposer (the finest searching solution). This procedure in some ways exemplifies exploitation.

$$\begin{aligned} AR_k(1 + Ti) = {} & AR_{Best}(Ti) + 3N(0, 1) \\ & \times [(z_3.z([1\ \ 2]) - 1))AR_{Best}(Ti) - (2z_3 - 1)AR_k(Ti)], \\ & k = 1{:}P_M \end{aligned} \tag{27}$$

B. ENHANCED EAEO: PROPOSED INTELLIGENT VERSION

The FDBM choosing technique's designing objective is to consistently and successfully select the people who would provide the most to the search procedures within a population. By using the Euclidean distance metric to compute the distance between each solution vector and the best individual associated with each iteration (AR_{Best}), it is ensured that the intensification and diversity operations are performed in a balanced manner. This approach enables the calculation of the distance of each member (DST_k) from the optimal choice. Specifically, the method for calculating the distance of each solution vector from the optimal choice is as follows:

$$DST_k = \sqrt{\sum_{m=1}^{D} \left(AR_{k,m} - AR_{Best,m}\right)^2}, \quad k = 1{:}P_M \tag{28}$$

In the second step of the FDBM approach, the grade for the different solutions is established. The grade derivation uses the candidates' normalized values for fitness (NFT) and normalized distance measures ($NDST$). They are able to be assessed in accordance with every individual (k) in the following manner:

$$NDST_k = \frac{DST_k - DST_{k,min}}{DST_{k,max-DST_{k,min}}}, \quad k = 1{:}P_M \tag{29}$$

$$NFT_k = \frac{FT_k - FT_{k,min}}{FT_{k,max-FT_{k,min}}}, \quad k = 1{:}P_M \tag{30}$$

In light of this, the employing of normalized quantities aims to impede both features from overpowering one another in the estimation of the objective. As a result, the following criteria may be used to evaluate every individual's grade (GRD):

$$GRD_k = NFT_k + NDST_k, \quad k = 1{:}P_M \tag{31}$$

After establishing each person's grade, a roulette wheel choice procedure [68] is used to find a solution that has a large probability of being graded highly (AR_{FDBM}). As a result, by using the FDBM approach, the decomposition step which is described in Eq. (27) can be improved as follows:

$$\begin{aligned} AR_k(1 + Ti) = {} & AR_{FDBM}(Ti) + 3N(0, 1) \\ & \times [(z_3.z([1\ \ 2]) - 1))AR_{Best}(Ti) - (2z_3 - 1)AR_k(Ti)], \\ & k = 1{:}P_M \end{aligned} \tag{32}$$

The proposed EAEO methodology as envisioned is shown in Figure 3. It starts by creating a population at random. The first person to search shifts its position in relation to Eq. (21)

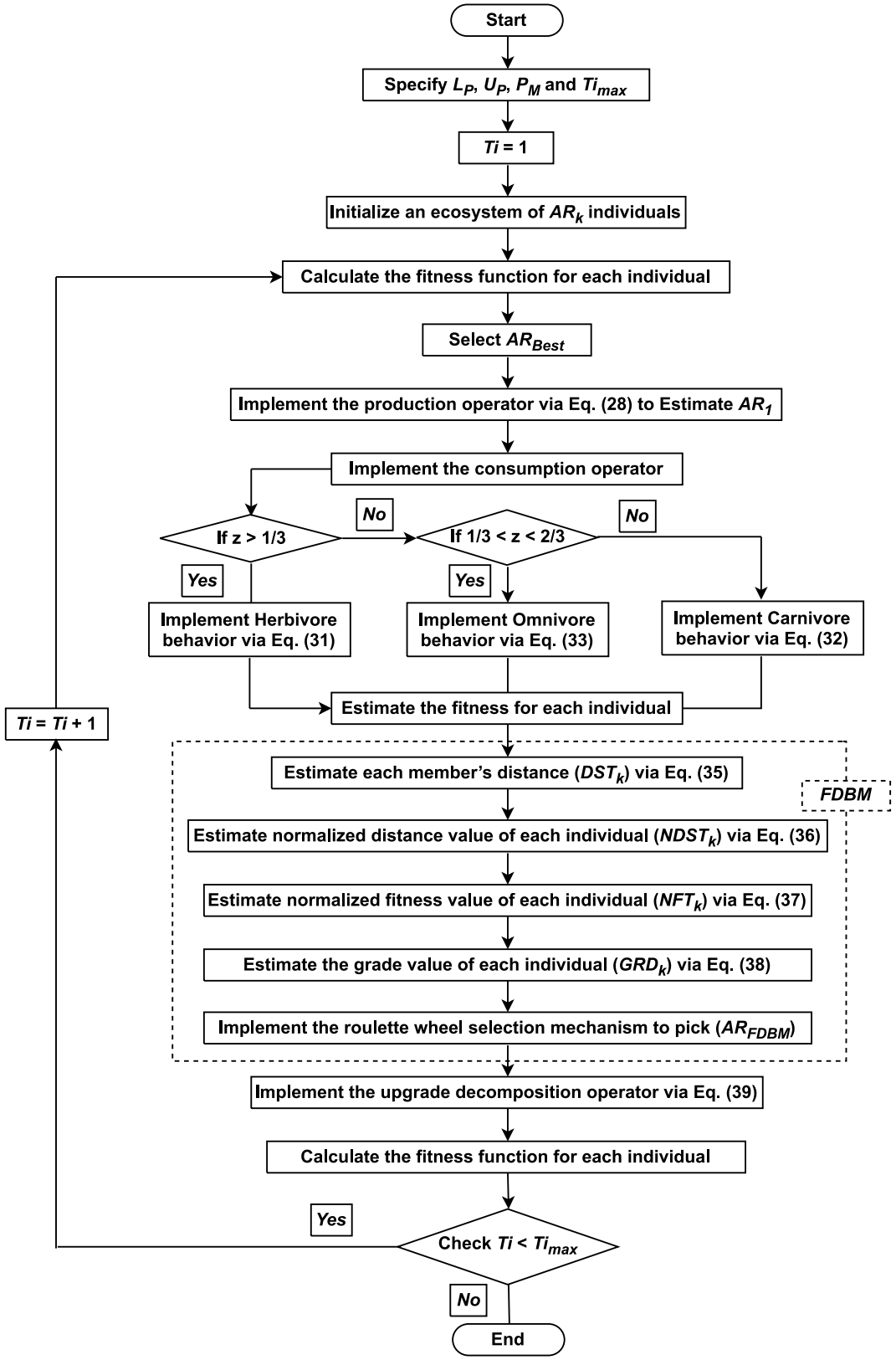

FIGURE 3. Key steps of the proposed EAEO version.

with each repeat, while the other people have an equal chance of selecting Herbivore in accordance with Eq. (24), Carnivore in accordance with Eq. (25), or Omnivore in accordance with Eq. (26) to alter their places. If an individual has a higher fitness trait, it might sound acceptable. The FDBM process is initiated to select a solution with a

high probability of achieving a good performance. This is accomplished by calculating the distance between each candidate solution and the optimal choice, as described in Eq. (28). Next, the normalized fitness and distance scores for the candidate search solutions are assessed using Eqs. (29) and (30), respectively. Finally, the grade for each candidate solution is determined using Eq. (31) in the second step of the FDBM approach.

Subsequently utilizing Eq. (32), each member's position could be modified. When the searching universe is far from the upper or lower borders during the modification stage, individuals are created independently. All changes are made constantly up until the EAEO technique finds the termination requirement. The choice of the best individual is attained in the end.

V. NUMERICAL RESULTS

This section presents the simulation results obtained from a variety of numerical tests. These tests show the advantages of RIS-enabled ISAC systems and shed light on the effectiveness of the suggested method. The simulation parameters used in the tests are as follows: the DFBS is located at (0,0,0) m, the comm-RIS is situated at (20,13,3) m, the radar-RIS is positioned at (–6,6,3) m, the target angles with respect to the DFBS are $(-70°,-50°,-30°,-20°,-10°)$, and the distance between the targets and the DFBS is 5m. A 100 MHz signal bandwidth and 30 GHz carrier frequency are used. This band is suited for use in very challenging communication situations, such as mountainous regions where it is challenging to mobilize BS with direct link due to the topography. Alternatively, the environment may change as a result of weather, natural disasters, etc., rendering the initial connection invalid. As a result, it is possible to accomplish communication and sensing more easily and at less money [69].

Large RISs with high carrier frequencies have a much larger near-field zone than existing systems (without RISs). To be able to get higher passive beamforming gains, it is preferable for RISs to be placed close to the transmitter or receiver. Consequently, in ISAC systems that make use of RIS, near-field communication and sensing will be used more frequently. Electromagnetic waves in the near-field needs to be modelled using a spherical wave, which may be focused on a certain distance as well as guided towards a specific angle, in contrast to the planar wave model used for transmission in the far-field. With the help of this approach, greater communication capabilities and more precise parameter estimation for sensing can be obtained. Nevertheless, it is evident that intricate beamforming and channel estimation solutions are required, especially when there are a large number of RIS reflecting components and BS transmit/receive antennas [70].

The simulation is divided into two sections. The communication system's SNR performance is shown in the first part. The effectiveness of the suggested EAEO optimisation algorithm is assessed in the second section. To illustrate RIS's benefits in ISAC systems We show results from the Monte-Carlo experiments for the two alternative scenarios with respect to the feasible SINR and worst-case illumination power at the target sites of interest. These outcomes were attained by adjusting a number of system parameters, including the number of RIS elements (N) and the SINR requirement (Γ).

In the first situation, we require the radar beam to have peaks towards target directions and the communication beam to have a stronger peak towards the RIS. This is preferred since the comm-RIS's main purpose is to service the UEs, and any radar emissions directed at the UEs via the RIS run the risk of increasing interference and lowering SINR at the UEs. In contrast to transmitting radar signals to UEs, which causes interference, transmitting communication signals toward the target actually aids in enhancing the target illumination strength, which explains the peaks of communication beams in that direction.

In the second case study, we show the benefits of utilizing specialised RISs for sensing and communications in an ISAC system. We suppose that two similar RIS with N elements support the ISAC system's communication and sensing capabilities. Here, we provide the worst-case target illumination power and fairness SINR (or min-rate) for a variety of simulation settings, including SINR constraints (Γ) and the number of RIS elements (N).

A. COMMUNICATION AND RADAR SYSTEMS

The performance of the communication system is tested using SNR. The simulations are performed using the proposed system model, where a ULA made up of 16 equally spaced half-wavelength pieces serves as a representation of a DFBS. Meanwhile, the comm-RIS and radar-RIS are modeled using URAs comprising quarter-wavelength spaced elements.The channels $\boldsymbol{F}_{br}, \boldsymbol{E}_{br}$, and $\boldsymbol{f}_{ru,k}^{H}$ are modelled as Rician distributed random variables, where $\rho = 10$ is the Rician factor. It is expected that the direct channel for communication UEs, which is $\boldsymbol{f}_{bu,k}^{H}$ for $k = 1, \ldots, K,$, will experience Rayleigh fading. LOS channels are modelled for the remaining channels, which are $\boldsymbol{e}_{bt,m}$ and $\boldsymbol{e}_{rt,m}$ for $m = 1, \ldots, T$. At the UEs, the receiver noise variance is set to -94 dBm.

The DFBS and radar-RIS are both believed to have targets in their far fields. The user locations are randomly drawn from a rectangular grid with corners at (15, 8, 0)m, (15, 18, 0)m, (18, 8, 0)m, and (18, 18, 0)m. This ensures that the users are distributed within a specific area of interest. The pathlosses are modeled as $(30+25)\log d$ dB and $(30+36)\log d$ dB for the radar-RIS-target links and the DFBS-UE links, respectively. The pathlosses for the remaining links are modeled as $(30+22)\log d$ dB, where d represents the distance in meters between the corresponding terminals.

This modeling is based on the assumption that the signal strength decreases with distance, and the pathlosses are calculated using a logarithmic function. By modeling the pathlosses in this way, the authors aim to accurately simulate

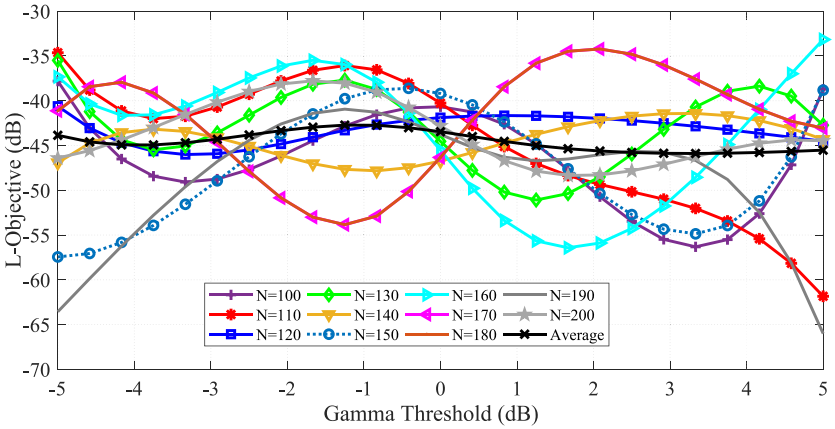

FIGURE 4. L-objective versus the Gamma threshold for different values of RIS elements $N = [100:10:200]$ and $\Gamma = [-5:5]dB$.

the real-world propagation characteristics of the signals in the ISAC system.

Figure 4 shows the relation between the L-objective on the y-axis and the Gamma threshold on the x-axis for different values of N, ranging from 100 to 200. Assuming the number of users $K = 4$, number of targets $T = 5$, $Q_t = 0$ dB, and number of RIS elements takes the values $N = \{100, 130, 160, 200\}$. The L-objective is a measure of the quality of the reconstructed signal and is used to evaluate the performance of the signal reconstruction algorithm. The lower the L-objective value, the better the reconstructed signal. The Gamma threshold is a parameter used in statistical hypothesis testing to determine the significance of a test result. In this case, it's being used to determine the presence or absence of a signal in the data. As the Gamma threshold increases, the algorithm becomes more sensitive to the presence of a signal, which typically leads to a better quality of the reconstructed signal. This is reflected in the plot by the increasing trend of the curves from right to left. The plot also shows that increasing the number of elements N generally leads to better reconstruction performance, as indicated by the increasing trend of the curves from bottom to top. This is because more elements provide more information about the underlying signal, making it easier to reconstruct. Finally, the average L-objective value across all values of N, indicates that the overall performance of the algorithm is quite good, with an average L-objective value of –44.51 dB. The oscillation proves that the proposed algorithm achieved the constraint under different values of Γ.

Figure 5 shows the impact of Γ on SNR for four users under different number of RIS elements N. For $N = 100$ and $\Gamma = 5$ dB, the SNR equal 21.14196349 dB, 20.323719 dB, 18.49051492 dB and 18.89608248 dB for User1, User2, User3 and User4 respectively. Furthermore, the impact of N on SNR is examined for the same users. Figure 6 shows that when $N = 130$, User1 achieves SNR value of 22.76848683 dB, whereas User2, User3, and User4 obtain SNR equal 20.85823979 dB, 20.63021313 dB, and 19.19838523 dB respectively. In Figure 7 when $N = 160$ the SNR equals 21.38471132 dB,

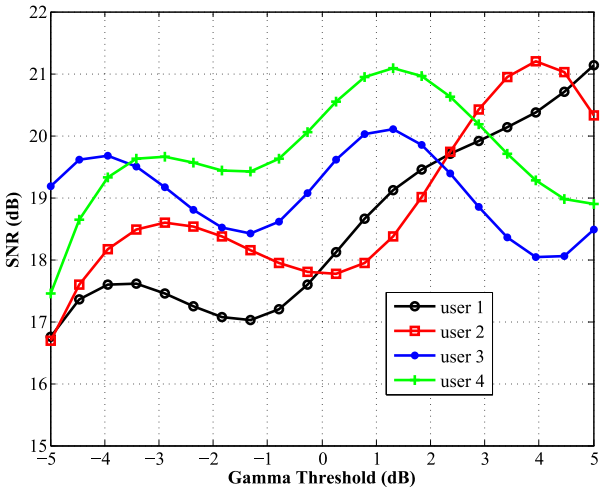

FIGURE 5. SNR versus Gamma Threshold for number of RIS elements N=100.

20.01564217 dB, 21.57417519 dB, and 21.31337402 dB for User1, User2, User3, and User4 respectively. Moreover, when $N = 200$, the SNR equals 23.26451717 dB, 22.47588875 dB, 25.34659153 dB, and 21.29472268 dB for User1, User2, User3, and User4, respectively as shown in Figure 8. In conclusion, increasing the number of RIS elements N, under the same Gamma threshold, increases the average SNR for each user.

Figure 9 shows the average convergence for the proposed EAEO algorithm as compare with different optimization algorithm.

B. VALIDATION TEST OF THE PROPOSED EAEO ALGORITHM

There are two sections in this part. The suggested EAEO is applied to 28 distinct mathematical benchmarking functions that are related to the IEEE CEC'17 test set. The suggested EAEO, original AEO [47] and a number of more modern metaheuristic algorithms, such as the SMA [55], ESMA [56], [57], GSO [58] and CO [59], are compared in order to evaluate how well the newer metaheuristic algorithms perform. The second part investigates

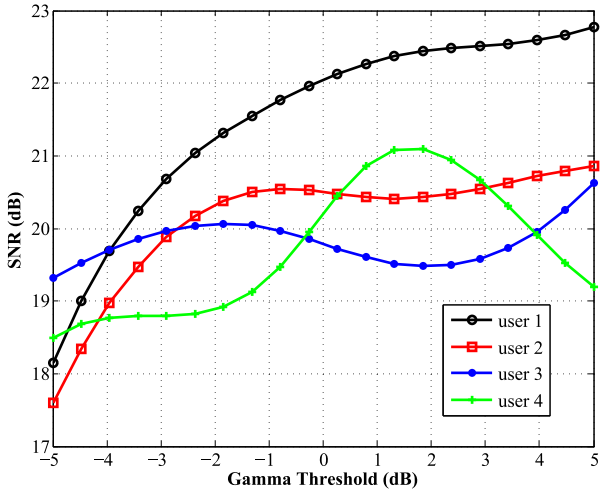

FIGURE 6. SNR versus Gamma Threshold for number of RIS elements N=130.

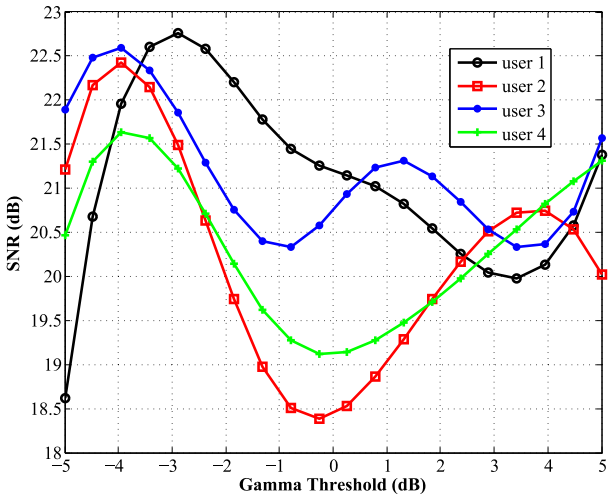

FIGURE 7. SNR versus Gamma Threshold for number of RIS elements N=160.

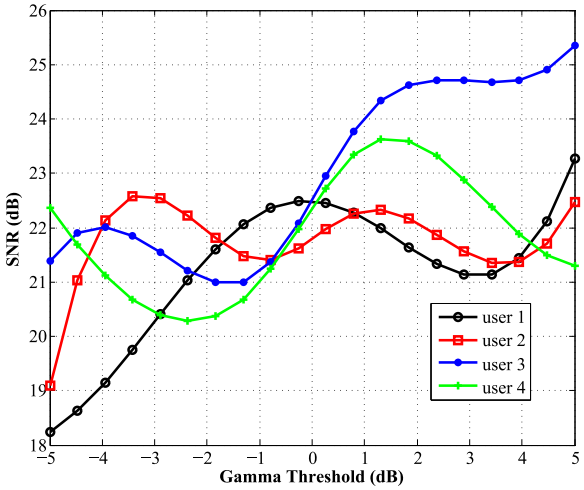

FIGURE 8. SNR versus Gamma Threshold for number of RIS elements N=200.

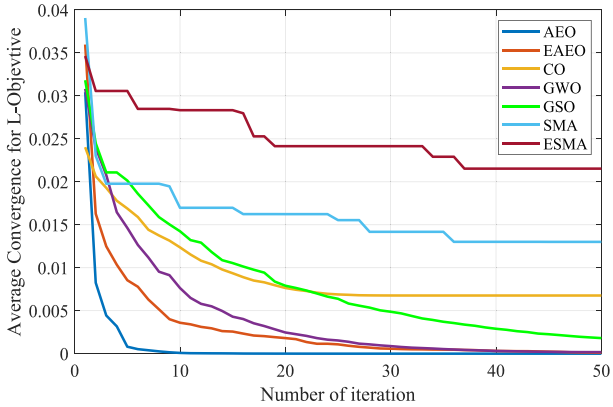

FIGURE 9. Average convergence for L-objective. There are different optimization algorithms AEO, EAEO, CO, GSO, SMA, and GWO. The number of BS antennas $M = 16$, number of RIS elements $N = 100$ and $\Gamma = 5dB$.

how the suggested EAEO for beamforming optimization framework might be used to integrate sensing and communication systems with changeable intelligent surfaces.

In the first part, numerous implementations of various numerical benchmarks are made using the proposed EAEO, the traditional AEO, SMA, ESMA, CO, and GSO. The efficacy of the proposed EAEO is assessed using CEC'17, which has been viewed as a challenging testbed because of its extreme complexity. Ten-dimensional CEC'17 functionalities are tested using the proposed EAEO. Following the elimination of F2, the CEC'17 test suite comprises 28 commonly used functions as reported by Liang et al. [71]. These functions are categorized into four groups: unimodal functions (F1 and F3), multimodal functions (F4–F10), hybrid functions (F11–F20), and combination functions (F21–F28).

Tables 1, 2 show the comparison between the EAEO proposed algorithm and other algorithms in achieving L-objective for the first scenario (Table 1) and Q-objective for the second scenario (Table 2). The tables show the superiority of EAEO over all other algorithms in terms of minimum L-objective and maximum Q-objective. Moreover, we simulate the comparison between different algorithms. Figure 10 shows that EAEO has the best performance in L-objective for different values of the number of RIS. Also, Figure 11 shows the highness of EAEO in terms of Q-objective.

Utilizing multimodal functions, the capacity to escape the immediate environment is evaluated. The trade-off between the exploitation and exploratory capacities of the search algorithms is investigated using composite functions representing real optimization problems with very dynamic search spaces. In order to provide an accurate assessment, the contrasting algorithms are put into effect using 30 agents for searching and 500 iterations. Their results are listed in Tables 1, 2, and 3, accordingly, in terms of the best, mean, and worst.[3]

In Tables 3, 4 and 5, the suggested EAEO outperforms the standard AEO, CO, GSO, SMA, and ESMA in terms of efficacy and robustness. For the best, mean, and worst

3. The convergence characteristics for the 28 benchmark functions are shown in the attached supplementary material.

TABLE 1. L-objective for different optimization algorithms AEO, EAEO, CO, GSO, SMA, and ESMA for number of BS antennas $M = 16$, $\Gamma = 5dB$, and number of RIS elements $N = \{100, 150, 200\}$.

	L-Objective (Best)					
	AEO	**EAEO**	**CO**	**GSO**	**SMA**	**ESMA**
N = 100	7.21668E-6	8.97139E-07	0.001516219	0.000991353	1.55032E-5	7.9148E-5
N = 150	3.59473E-6	2.1179E-07	0.0001812651	0.000760871	2.52353E-6	1.4243E-6
N = 200	2.17965E-7	7.61342E-08	0.0000194842	0.0000981912	6.33234E-7	2.32657E-7
	L-Objective (Mean)					
	AEO	**EAEO**	**CO**	**GSO**	**SMA**	**ESMA**
N = 100	1.3605E-3	0.000108822	0.006767586	0.001810984	0.013010762	0.021534442
N = 150	2.9727E-4	7.72419E-05	0.006443172	0.001875231	0.006740556	0.0075672
N = 200	1.69302E-5	3.18351E-06	0.0008641025	0.000873487	0.001629419	0.0014987
	L-Objective (Worst)					
	AEO	**EAEO**	**CO**	**GSO**	**SMA**	**ESMA**
N = 100	1.07814E-3	0.000458413	0.022362992	0.003564935	0.045953952	0.056610861
N = 150	5.39611E-4	0.000233308	0.01855605	0.002978161	0.005575339	0.032241
N = 200	2.65202E-4	0.000134898	0.0024550518	0.002743097	0.0038199864	0.00456328

TABLE 2. Q-objective for different optimization algorithms AEO, EAEO, CO, GSO, SMA, and ESMA for number of BS antennas $M = 16$, $\Gamma = 5dB$, and number of RIS elements $N = \{100, 150, 200\}$.

	Q-Objective (dB) (Best)					
	AEO	**EAEO**	**CO**	**GSO**	**SMA**	**ESMA**
N = 100	26.69133206	31.00935499	20.83820783	29.63951457	29.84714661	30.00935499
N = 150	28.08705009	32.46005859	24.60694265	30.44925425	30.1024557	31.46005859
N = 200	30.024465	33.781245	25.93913921	31.23264547	32.60539505	32.1014526
	Q-Objective (dB) (Mean)					
	AEO	**EAEO**	**CO**	**GSO**	**SMA**	**ESMA**
N = 100	23.34934698	27.55736226	16.68657552	27.36515904	26.72133075	26.55736226
N = 150	25.37335222	29.57151724	18.72374168	28.90128826	28.55671102	28.57151724
N = 200	27.8365798	31.2144577	19.58049588	30.06454553	30.11194594	30.2645025
	Q-Objective (dB) (Worst)					
	AEO	**EAEO**	**CO**	**GSO**	**SMA**	**ESMA**
N = 100	19.93505742	24.6505616	10.00127884	22.75463115	23.92911588	23.6505616
N = 150	23.14441585	25.24629627	12.80101778	23.29920675	24.0442168	24.24629627
N = 200	26.2465887	26.7456772	15.57426696	25.23614459	25.68952856	25.2664245

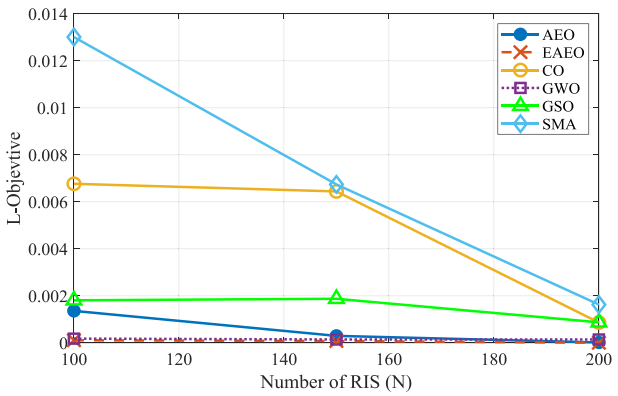

FIGURE 10. L-objective versus number of RIS elements (N) for different optimization algorithms AEO, EAEO, CO, GSO, SMA, and ESMA. The number of BS antennas $M = 16$, $\Gamma = 5dB$, and number of RIS elements $N = \{100, 150, 200\}$.

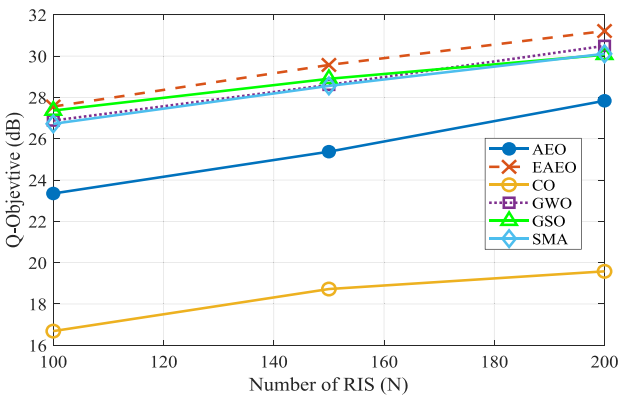

FIGURE 11. Q-objective versus number of RIS elements (N) for different optimization algorithms AEO, EAEO, CO, GSO, SMA, and ESMA. The number of BS antennas $M = 16$, $\Gamma = 5dB$, and number of RIS elements $N = \{100, 150, 200\}$.

of the acquired fitness, the recommended EAEO surpasses the traditional AEO in 70%, 86.87%, and 83.33% of the benchmark functions, respectively. The suggested EAEO surpasses the CO for the best, mean, and worst of the obtained fitness, respectively, in 96.43%, 100%, and 100% of the benchmark functions.Compared to the GSO, the

TABLE 3. Obtained best of EAEO, AEO, CO, GSO, SMA, and ESMA for the 28 benchmark functions.

Function name	Best					
	EAEO	AEO	CO	GSO	SMA	ESMA
F1	**101.2**	110.56	130840.00	48532.00	115.64	100.38
F2	**300**	**300**	3631.00	862.84	**300.00**	**300.00**
F3	400.15	**400**	501.24	404.19	400.05	400.01
F4	**502.99**	509.95	551.75	519.12	503.98	505.97
F5	**600.01**	605.88	633.65	614.06	600.08	600.04
F6	**709.59**	724.92	771.23	739.97	715.20	712.85
F7	**802.98**	811.94	833.54	816.01	804.98	806.97
F8	**900**	918.09	1049.20	1007.40	**900.00**	**900.00**
F9	**1006.9**	1224.1	1898.30	1621.20	1168.70	1165.30
F10	**1100.3**	1102	1233.00	1116.00	1103.40	1101.00
F11	2003	**1775.7**	1662800.00	3612.70	5561.40	3253.40
F12	**1310.3**	1343.7	190570.00	1679.70	1465.10	1319.60
F13	**1402.4**	1421	1740.20	1446.60	1435.00	1434.10
F14	**1502.1**	1502.6	3271.00	1713.10	1522.30	1504.70
F15	**1600.6**	1600.9	1775.30	1675.80	1602.10	1601.80
F16	**1703.5**	1725.2	1774.90	1750.60	1721.00	1705.50
F17	**1815.9**	1834.4	326110.00	1949.00	3473.40	2166.90
F18	**1902**	1905.4	5104.50	1935.80	1908.00	1915.70
F19	**2001**	2004.6	2161.40	2068.10	2005.30	2004.00
F20	**2200**	**2200**	2220.40	2204.60	2202.80	**2200.00**
F21	**2200**	2234.2	2436.00	2308.10	2241.00	2300.50
F22	**2605**	2617	2621.30	2625.10	2612.40	2607.40
F23	**2500**	**2500**	2608.40	2524.40	2734.70	2735.40
F24	**2897.7**	2897.9	2971.10	2901.50	2898.20	2897.80
F25	2900	**2800**	3166.90	2848.80	2816.00	2800.20
F26	3090.4	3095	3105.40	3103.70	**3089.00**	**3089.00**
F27	**3100**	**3100**	3341.20	3176.30	3167.50	3166.50
F28	3140.7	3150.4	3171.20	3189.20	3134.40	**3134.40**

suggested EAEO outperforms it in 100%, 100%, and 100% of the benchmark functions for the best, mean, and worst of the acquired fitness, respectively. Compared to the SMA, the suggested EAEO outperforms it in 85.71%, 92.85%, and 92.85% of the benchmark functions for the best, mean, and worst of the acquired fitness, respectively.

Compared to the ESMA, the suggested EAEO outperforms it in 82.17%, 85.71%, and 60.71% of the benchmark functions for the best, mean, and worst of the acquired fitness, respectively.

To sum up, simulation results have demonstrated that integrated RIS in ISAC systems can accomplish highly accuracy, wide coverage, and high reliable sensing and communication features. These capabilities will be crucial in advancing the development of future 6G networks. Through skilled manipulation of the propagation environment, the receiver can localize and produce an accurate radio map by exploiting the variations in signals reflected from various targets or places. Furthermore, as the BS is typically situated beyond the radar's guard zone to safeguard it from unwanted interference, the implementation of RIS facilitates coverage for users within the radar exclusion zone and enhances the quality of communication services (QoS). In addition, new prospects for conventional sensing applications arise with the implementation of RIS. Deploying RIS can enhance the sensing performance for targets that already enjoy LoS propagation and enable the radar to sense targets in shadowed areas that would normally be invisible to it. This is achieved by creating an effective LoS link and providing additional degrees of freedoms (DoFs) for optimization.

The computer resources utilized by the optimization method to acquire a solution are referred to as the time complexity of the comparing algorithms. A variety of factors may impact this difficulty, including the dimensions of the problem, the overall number of repetitions, and the degree of complexity of the objective assessment function. Assessing the time complexity of the examined algorithms entails comprehending the number of fitness evaluations required

TABLE 4. Obtained mean of EAEO, AEO, CO, GSO, SMA, and ESMA for the 28 benchmark functions.

Function name	Mean					
	EAEO	AEO	CO	GSO	SMA	ESMA
F1	**1464.2**	1957.7	389590.00	132910.00	4047.10	3042.80
F2	300.05	**300**	7192.00	14241.00	300.05	300.09
F3	403.06	**402.83**	714.73	506.25	407.54	405.41
F4	**512.19**	540.43	579.45	561.92	514.89	515.62
F5	**600.05**	618.29	646.92	645.26	600.17	600.09
F6	**723.07**	765.97	796.06	789.00	725.50	724.81
F7	**811.73**	828.54	850.81	846.86	816.62	814.53
F8	900.06	1086.3	1403.00	1631.00	900.25	**900.00**
F9	1489.3	2019.2	2727.50	2610.20	1511.80	**1462.20**
F10	**1106.7**	1142.9	1659.30	2006.00	1137.80	1112.40
F11	**9626.8**	16902	131410.00	248790.00	207930.00	21345.00
F12	**1399.2**	1816.8	329250.00	108430.00	8132.90	2161.80
F13	**1422.9**	1484.7	5668.90	3889.00	1929.00	1764.30
F14	**1520.3**	1591.9	11877.00	18439.00	3349.90	4320.80
F15	**1609.9**	1786.8	2070.70	2083.80	1663.50	1646.50
F16	**1724.7**	1778.4	1811.90	1889.90	1747.10	1730.10
F17	**1882.2**	3930.8	75619.00	502870.00	19428.00	24256.00
F18	**1907.5**	1951.5	229180.00	726860.00	5501.10	3553.30
F19	**2013.1**	2092.2	2250.60	2268.90	2030.30	2021.80
F20	**2205.2**	2246.1	2329.20	2341.70	2304.40	2313.90
F21	**2295.8**	2302	2632.50	2417.30	2298.10	2301.90
F22	**2615.3**	2654.3	2687.20	2718.90	2619.50	2616.50
F23	**2633.8**	2719.6	2792.70	2822.50	2751.60	2751.00
F24	**2922.3**	2923.3	3155.50	2971.40	2922.20	2917.80
F25	**2901.2**	3056.8	3494.10	3667.10	3022.60	2953.30
F26	**3096.1**	3123.5	3154.90	3174.10	3090.50	3091.00
F27	**3111.5**	3274.4	3587.20	3478.50	3320.00	3342.20
F28	**3163.7**	3258.6	3422.50	3384.80	3186.20	3180.70

and how it scales with problem size. The complexity of all examined algorithms is fixed, allowing for a fair comparison. The complexity of each algorithm equal $O(150,000) \times O(F(x))$ for 30 solution, 500 iteration, and dimension of 10.

There are different structures of joint communication and sensing (JCAS) combined with cutting-edge technologies (such as cloud radio access networks, unmanned aerial vehicles, and RISs). In the first structure, distributed nodes are used to transmit or receive signals, and these signals are collaboratively processed in a central unit. This is known as JCAS with cooperative MIMO. Here, each node can be assigned to communication-only, sensing-only, or both. In addition to enhancing individual communication and sensing performance, macro diversity provides additional options for the system to design the two tasks in a more compatible way. The crucial issue, which requires careful consideration, is the flexible orchestration of several nodes and their roles. This involves intricate connections between various nodes in terms of rivalry and cooperation [72]. In the second structure, UAVs are added to the network for sensing and communication. The BS view for sensing is limited by the fact that terrestrial BSs' antennas are angled downward to cover ground users. When the UAV is near the target or the user, the directional beam can be utilized to enhance the communication rate or fine-tune the sensing resolution. When the UAV is flying high, the wide sensing beam can be utilized to illuminate the entire region. In this instance, DoFs are used in both the spatial and temporal domains by the JCAS using UAVs. While the joint optimization in the temporal and spatial domains doubles the degrees of freedom, it also increases the complexity of the optimization exponentially. Moreover, simple design is necessary due to UAVs' energy and hardware constraints [73]. The final one enhances communication and sensing capabilities by integrating passive and active MIMO (also known as RIS) into the JCAS network. It adds both significant complexity and DoFs. The RIS aids in improving the waveform that the node only produces when it is of low quality. It modifies

TABLE 5. Obtained worst of EAEO, AEO, CO, GSO, SMA, and ESMA for the 28 benchmark functions.

Function name	Worst					
	EAEO	AEO	CO	GSO	SMA	ESMA
F1	9065	11309	92394.0	28897.0	12677.00	**5542.40**
F2	**300.27**	300.03	10628.0	78883.0	300.35	300.39
F3	405.37	**405.33**	1006.7	1547.1	456.99	407.21
F4	525.87	584.57	611.5	623.22	530.26	**521.49**
F5	600.28	645.38	662.27	678.05	600.51	**600.12**
F6	741.17	807.73	818.59	880.06	742.81	**731.80**
F7	832.83	852.73	863.56	923.48	829.85	**820.90**
F8	900.8	1776.7	1677.1	4350.50	905.83	**900.00**
F9	**1960.2**	2735.4	3020.8	3664.50	1980.10	1679.00
F10	**1117.8**	1241.4	3062.2	17767	1336.50	1124.30
F11	53967	**52529**	2363500	2418100	1267400.0	597810.0
F12	**1663.6**	6936.3	186570	270800	32548.00	4041.90
F13	**1442.5**	1885	29799.0	28906	8381.60	2504.00
F14	**1564.7**	2237	20748.0	103090	11424.00	7356.10
F15	**1721.5**	2007.2	2283.20	2769.8	1899.60	1731.60
F16	**1747.7**	1886.8	1850.10	2217.90	1838.80	1747.80
F17	**2102.9**	34619	255060	125660	42539.00	35618.00
F18	**1935**	2177.4	973510	198640	28127.00	13985.00
F19	2037.8	2238.5	2386.0	2693.20	2073.60	**2036.50**
F20	**2314.2**	2372.7	2413.7	2413.90	2335.40	2328.90
F21	2303.6	2318.9	2979.9	3791.10	2304.20	**2302.90**
F22	2627.7	2700.8	2755.2	2901.10	2633.50	**2623.60**
F23	2758	2817.9	2923.0	2992.40	2772.20	**2762.70**
F24	**2945.9**	2952.3	3382.3	3179.20	2969.40	2947.00
F25	**2959.3**	3460.9	4128.6	4859.70	3920.70	2999.10
F26	3117.5	3206.7	3219.6	3312.60	3095.30	**3092.70**
F27	**3383.8**	3446.5	3750.1	4019.00	3731.80	3411.80
F28	**3208.1**	3441.6	3663.2	3757.00	3283.50	3235.30

its components to suppress the sidelobes and magnify the mainlobes. Consequently, the initially indistinguishable beam is reshaped and take on the appearance of a hand with distinct sub-beams. Both target identification and user separability have significantly increased.

VI. CONCLUSION

In this paper, two different advanced scenarios of RIS-assisted ISAC systems are investigated: 1) One RIS is used, and it only supports communication functionality, and 2) Two RISs are dedicated and used for sensing and communication. In this paper, an advanced EAEO technique is proposed to build transmit beamformers and RIS phase shifts. Therefore, communication symbols and radar waveforms are jointly pre-coded in order to achieve a specific level of sensing performance and ensure adequate SNR for communication users. In this regard, an intelligent EAEO version involving an FDBM is presented to improve the quality of the solutions in multidimensional and nonlinear optimization scenarios. The proposed EAEO is tested on 28 different numerical benchmark functions related to the IEEE CEC'17 test suite. The effectiveness of the simulation results in solving the CEC'17 test suite is assessed. A comparative analysis is conducted compared to the standard AEO and several recent metaheuristic algorithms including SMA, ESMA, CO and GSO. The simulations demonstrate the suggested EAEO's superior effectiveness and resilience to the standard AEO and SMA, ESMA, CO, and GSO. The results showed that the proposed technique had a higher rate of success in achieving the global optimum point. The proposed EAEO has shown promise in its capacity to solve issues. Numerical simulations illustrate how well the proposed algorithm performs. The ISAC system with comm-RIS support considerably increased fairness SNR at the expense of a modest reduction in radar performance. Contrarily, all communication and radar performance metrics were significantly enhanced by the dual-RIS-aided ISAC system. These findings imply that the wireless communication and sensing capabilities of ISAC

systems with RIS assistance may be enhanced in a variety of contexts.

REFERENCES

[1] J. A. Zhang et al., "Enabling joint communication and radar sensing in mobile networks–A survey," *IEEE Commun. Surveys Tuts.*, vol. 24, no. 1, pp. 306–345, 1st Quart., 2022.

[2] F. Liu, C. Masouros, A. P. Petropulu, H. Griffiths, and L. Hanzo, "Joint radar and communication design: Applications, state-of-the-art, and the road ahead," *IEEE Trans. Commun.*, vol. 68, no. 6, pp. 3834–3862, Jun. 2020.

[3] V. W. Wong, R. Schober, D. W. K. Ng, and L.-C. Wang, *Key Technologies for 5G Wireless Systems*. Cambridge, U.K.: Cambridge Univ. Press, 2017.

[4] A. Liu et al., "A survey on fundamental limits of integrated sensing and communication," *IEEE Commun. Surveys Tuts.*, vol. 24, no. 2, pp. 994–1034, 2nd Quart., 2022.

[5] F. Liu et al., "Integrated sensing and communications: Toward dual-functional wireless networks for 6G and beyond," *IEEE J. Sel. Areas Commun.*, vol. 40, no. 6, pp. 1728–1767, Jun. 2022.

[6] L. Zheng, M. Lops, Y. C. Eldar, and X. Wang, "Radar and communication coexistence: An overview: A review of recent methods," *IEEE Signal Process. Mag.*, vol. 36, no. 5, pp. 85–99, Sep. 2019.

[7] M. Labib, V. Marojevic, A. F. Martone, J. H. Reed, and A. I. Zaghloui, "Coexistence between communications and radar systems: A survey," *URSI Radio Sci. Bull.*, vol. 2017, no. 362, pp. 74–82, Sep. 2017.

[8] M. Di Renzo et al., "Smart radio environments empowered by reconfigurable intelligent surfaces: How it works, state of research, and the road ahead," *IEEE J. Sel. Areas Commun.*, vol. 38, no. 11, pp. 2450–2525, Nov. 2020.

[9] Y. Cao, S. Xu, J. Liu, and N. Kato, "IRS backscatter enhancing against jamming and eavesdropping attacks," *IEEE Internet Things J.*, vol. 10, no. 12, pp. 10740–10751, Jun. 2023.

[10] Z. Xu, F. Liu, and A. Petropulu, "Cramér-Rao bound and antenna selection optimization for dual radar-communication design," in *Proc. IEEE Int. Conf. Acoust., Speech Signal Process. (ICASSP)*, 2022, pp. 5168–517.

[11] P. M. McCormick, S. D. Blunt, and J. G. Metcalf, "Simultaneous radar and communications emissions from a common aperture, part I: Theory," in *Proc. IEEE Radar Conf. (RadarConf)*, 2017, pp. 1685–1690.

[12] F. Liu, C. Masouros, A. Li, H. Sun, and L. Hanzo, "MU-MIMO communications with MIMO radar: From co-existence to joint transmission," *IEEE Trans. Wireless Commun.*, vol. 17, no. 4, pp. 2755–2770, Apr. 2018.

[13] C. Xu, B. Clerckx, S. Chen, Y. Mao, and J. Zhang, "Rate-splitting multiple access for multi-antenna joint radar and communications," *IEEE J. Sel. Topics Signal Process.*, vol. 15, no. 6, pp. 1332–1347, Nov. 2021.

[14] M. Roberton and E. Brown, "Integrated radar and communications based on chirped spread-spectrum techniques," in *IEEE MTT-S Int. Microw. Symp. Dig.*, vol. 1, 2003, pp. 611–614.

[15] G. N. Saddik, R. S. Singh, and E. R. Brown, "Ultra-wideband multifunctional communications/radar system," *IEEE Trans. Microw. Theory Tech.*, vol. 55, no. 7, pp. 1431–1437, Jul. 2007.

[16] K. V. Mishra, M. Bhavani Shankar, V. Koivunen, B. Ottersten, and S. A. Vorobyov, "Toward millimeter-wave joint radar communications: A signal processing perspective," *IEEE Signal Process. Mag.*, vol. 36, no. 5, pp. 100–114, Sep. 2019.

[17] X. Liu, T. Huang, N. Shlezinger, Y. Liu, J. Zhou, and Y. C. Eldar, "Joint transmit beamforming for multiuser MIMO communications and MIMO radar," *IEEE Trans. Signal Process.*, vol. 68, pp. 3929–3944, Jun. 2020. [Online]. Available: https://doi.org/10.1109/TSP.2020.3004739

[18] E. Basar, M. Di Renzo, J. De Rosny, M. Debbah, M.-S. Alouini, and R. Zhang, "Wireless communications through reconfigurable intelligent surfaces," *IEEE Access*, vol. 7, pp. 116753–116773, 2019.

[19] H. Wymeersch and B. Denis, "Beyond 5G wireless localization with reconfigurable intelligent surfaces," in *Proc. IEEE Int. Conf. Commun. (ICC)*, 2020, pp. 1–6.

[20] S. Buzzi, E. Grossi, M. Lops, and L. Venturino, "Foundations of MIMO radar detection aided by reconfigurable intelligent surfaces," *IEEE Trans. Signal Process.*, vol. 70, pp. 1749–1763, 2022.

[21] X. Wang, Z. Fei, Z. Zheng, and J. Guo, "Joint waveform design and passive beamforming for RIS-assisted dual-functional radar-communication system," *IEEE Trans. Veh. Technol.*, vol. 70, no. 5, pp. 5131–5136, May 2021.

[22] Z. Zhang et al., "Active RIS vs. passive RIS: Which will prevail in 6G?" *IEEE Trans. Commun.*, vol. 71, no. 3, pp. 1707–1725, Mar. 2023.

[23] L. Dong, H.-M. Wang, and J. Bai, "Active reconfigurable intelligent surface aided secure transmission," *IEEE Trans. Veh. Technol.*, vol. 71, no. 2, pp. 2181–2186, Feb. 2022.

[24] X. Wang, Z. Fei, J. Guo, Z. Zheng, and B. Li, "RIS-assisted spectrum sharing between MIMO radar and MU-MISO communication systems," *IEEE Wireless Commun. Lett.*, vol. 10, no. 3, pp. 594–598, Mar. 2021.

[25] R. S. Prasobh Sankar, B. Deepak, and S. P. Chepuri, "Joint communication and radar sensing with reconfigurable intelligent surfaces," in *Proc. IEEE 22nd Int. Workshop Signal Process. Adv. Wireless Commun. (SPAWC)*, 2021, pp. 471–475.

[26] Z.-M. Jiang et al., "Intelligent reflecting surface aided dual-function radar and communication system," *IEEE Syst. J.*, vol. 16, no. 1, pp. 475–486, Mar. 2022.

[27] Y. He, Y. Cai, H. Mao, and G. Yu, "RIS-assisted communication radar coexistence: Joint beamforming design and analysis," *IEEE J. Sel. Areas Commun.*, vol. 40, no. 7, pp. 2131–2145, Jul. 2022.

[28] X. Song, D. Zhao, H. Hua, T. X. Han, X. Yang, and J. Xu, "Joint transmit and reflective beamforming for IRS-assisted integrated sensing and communication," in *Proc. IEEE Wireless Commun. Netw. Conf. (WCNC)*, 2022, pp. 189–194.

[29] R. Liu, M. Li, and A. L. Swindlehurst, "Joint beamforming and reflection design for RIS-assisted ISAC systems," in *Proc. 30th Eur. Signal Process. Conf. (EUSIPCO)*, 2022, pp. 997–1001.

[30] R. Liu, M. Li, Y. Liu, Q. Wu, and Q. Liu, "Joint transmit waveform and passive beamforming design for RIS-aided DFRC systems," *IEEE J. Sel. Topics Signal Process.*, vol. 16, no. 5, pp. 995–1010, Aug. 2022.

[31] Z. Zhu et al., "Intelligent reflecting surface assisted integrated sensing and communications for mmWave channels," 2022, *arXiv:2202.00552*.

[32] E. Shtaiwi, H. Zhang, A. Abdelhadi, and Z. Han, "Sum-rate Maximization for RIS-assisted radar and communication coexistence system," in *Proc. IEEE Glob. Commun. Conf. (GLOBECOM)*, 2021, pp. 1–6.

[33] M. Hua, Q. Wu, C. He, S. Ma, and W. Chen, "Joint active and passive beamforming design for IRS-aided radar-communication," *IEEE Trans. Wireless Commun.*, vol. 22, no. 4, pp. 2278–2294, Apr. 2023.

[34] X. Wang, Z. Fei, J. A. Zhang, J. Huang, and J. Yuan, "Constrained utility maximization in dual-functional radar-communication multi-UAV networks," *IEEE Trans. Commun.*, vol. 69, no. 4, pp. 2660–2672, Apr. 2021.

[35] W. Chen, L. Li, Z. Chen, T. Quek, and S. Li, "Enhancing THz/mmWave network beam alignment with integrated sensing and communication," *IEEE Commun. Lett.*, vol. 26, no. 7, pp. 1698–1702, Jul. 2022.

[36] C. Chaccour, M. N. Soorki, W. Saad, M. Bennis, P. Popovski, and M. Debbah, "Seven defining features of Terahertz (THz) wireless systems: A fellowship of communication and sensing," *IEEE Commun. Surveys Tuts.*, vol. 24, no. 2, pp. 967–993, 2nd Quart., 2022.

[37] C. Chaccour, W. Saad, M. Debbah, and H. V. Poor, "Joint sensing, communication, and AI: A Trifecta for resilient THz user experiences," 2023, *arXiv:2305.00135*.

[38] B. Dawidowicz, P. Samczynski, M. Malanowski, J. Misiurewicz, and K. S. Kulpa, "Detection of moving targets with multichannel airborne passive radar," *IEEE Aerosp. Electron. Syst. Mag.*, vol. 27, no. 11, pp. 42–49, Nov. 2012.

[39] J. E. Palmer, H. A. Harms, S. J. Searle, and L. Davis, "DVB-T passive radar signal processing," *IEEE Trans. Signal Process.*, vol. 61, no. 8, pp. 2116–2126, Apr. 2013.

[40] E. C. Strinati et al., "Wireless environment as a service enabled by reconfigurable intelligent surfaces: The RISE-6G perspective," in *Proc. Joint Eur. Conf. Netw. Commun. 6G Summit (EuCNC/6G Summit)*, 2021, pp. 562–567.

[41] H. Kuschel, D. Cristallini, and K. E. Olsen, "Tutorial: Passive radar tutorial," *IEEE Aerosp. Electron. Syst. Mag.*, vol. 34, no. 2, pp. 2–19, Feb. 2019.

[42] A. Aubry, A. De Maio, and M. Rosamilia, "Reconfigurable intelligent surfaces for N-LOS radar surveillance," *IEEE Trans. Veh. Technol.*, vol. 70, no. 10, pp. 10735–10749, Oct. 2021.
[43] A. Sume et al., "Radar detection of moving targets behind corners," *IEEE Trans. Geosci. Remote Sens.*, vol. 49, no. 6, pp. 2259–2267, Jun. 2011.
[44] O. Rabaste, E. Colin-Koeniguer, D. Poullin, A. Cheraly, J.-F. Pétex, and H.-K. Phan, "Around-the-corner radar: Detection of a human being in non-line of sight," *IET Radar, Sonar Navig.*, vol. 9, no. 6, pp. 660–668, Jul. 2015.
[45] D. Tahmoush, J. Silvious, and B. Bender, "Radar surveillance in urban environments," in *Proc. IEEE Radar Conf.*, 2012, pp. 0220–0225.
[46] K.-P.-H. Thai et al., "Detection–Localization algorithms in the around-the-corner radar problem," *IEEE Trans. Aerosp. Electron. Syst.*, vol. 55, no. 6, pp. 2658–2673, Dec. 2019.
[47] W. Zhao, L. Wang, and Z. Zhang, "Artificial ecosystem-based optimization: A novel nature-inspired meta-heuristic algorithm," *Neural Comput. Appl.*, vol. 32, pp. 9383–9425, Jul. 2020.
[48] M. M. Elkholy, M. A. El-Hameed, and A. A. El-Fergany, "Artificial ecosystem-based optimiser to electrically characterise PV generating systems under various operating conditions reinforced by experimental validations," *IET Renew. Power Gener.*, vol. 15, no. 3, pp. 701–715, Feb. 2021.
[49] Y. Niu, X. Yan, Y. Wang, and Y. Niu, "Three-dimensional UCAV path planning using a novel modified artificial ecosystem optimizer," *Expert Syst. Appl.*, May 2023, Art. no. 119499.
[50] N. Van Thieu, S. D. Barma, T. Van Lam, O. Kisi, and A. Mahesha, "Groundwater level modeling using augmented artificial ecosystem optimization," *J. Hydrol.*, vol. 617, Feb. 2023, Art. no. 129034.
[51] A. Mahdy, R. El-Sehiemy, A. Shaheen, A. Ginidi, and Z. Elbarbary, "An improved artificial ecosystem algorithm for economic dispatch with combined heat and power units," *Appl. Sci.*, vol. 12, no. 22, 2022, Art. no. 11773.
[52] A. Shaheen, A. Elsayed, A. Ginidi, R. El-Sehiemy, and E. Elattar, "Reconfiguration of electrical distribution network-based DG and capacitors allocations using artificial ecosystem optimizer: Practical case study," *Alexandria Eng. J.*, vol. 61, no. 8, pp. 6105–6118, Aug. 2022.
[53] R. M. Rizk-Allah and A. A. El-Fergany, "Artificial ecosystem optimizer for parameters identification of proton exchange membrane fuel cells model," *Int. J. Hydrogen Energy*, vol. 46, no. 75, pp. 37612–37627, Oct. 2021.
[54] Y. Sonmez, S. Duman, H. T. Kahraman, M. Kati, S. Aras, and U. Guvenc, "Fitness-distance balance based artificial ecosystem optimisation to solve transient stability constrained optimal power flow problem," *J. Exp. Theor. Artif. Intell.*, early access, Jul. 26, 2022, doi: 10.1080/0952813X.2022.2104388.
[55] S. Li, H. Chen, M. Wang, A. A. Heidari, and S. Mirjalili, "Slime mould algorithm: A new method for stochastic optimization," *Future Gener. Comput. Syst.*, vol. 111, pp. 300–323, Oct. 2020.
[56] S. Sarhan, A. M. Shaheen, R. A. El-Sehiemy, and M. Gafar, "An enhanced slime mould optimizer that uses chaotic behavior and an elitist group for solving engineering problems," *Mathematics*, vol. 10, no. 12, p. 1991, 2022.
[57] S. Abid et al., "Development of slime mold optimizer with application for tuning cascaded PD-PI controller to enhance frequency stability in power systems," *Mathematics*, vol. 11, no. 8, p. 1796, 2023.
[58] M. Noroozi, H. Mohammadi, E. Efatinasab, A. Lashgari, M. Eslami, and B. Khan, "Golden search optimization algorithm," *IEEE Access*, vol. 10, pp. 37515–37532, 2022.
[59] M. H. Qais, H. M. Hasanien, R. A. Turky, S. Alghuwainem, M. Tostado-Véliz, and F. Jurado, "Circle search algorithm: A geometry-based metaheuristic optimization algorithm," *Mathematics*, vol. 10, no. 10, p. 1626, 2022.
[60] X. Li et al., "Integrated sensing, communication, and computation over-the-air: MIMO beamforming design," *IEEE Trans. Wireless Commun.*, vol. 22, no. 8, pp. 5383–5398, Aug. 2023.
[61] H. Hua, J. Xu, and T. X. Han, "Optimal transmit beamforming for integrated sensing and communication," *IEEE Trans. Veh. Technol.*, vol. 72, no. 8, pp. 10588–10603, Aug. 2023.
[62] J. Yao, J. Xu, W. Xu, D. W. K. Ng, C. Yuen, and X. You, "Robust beamforming design for RIS-aided cell-free systems with CSI uncertainties and capacity-limited backhaul," *IEEE Trans. Commun.*, vol. 71, no. 8, pp. 4636–4649, Aug. 2023.
[63] N. T. Nguyen, Q.-D. Vu, K. Lee, and M. Juntti, "Hybrid relay-reflecting intelligent surface-assisted wireless communications," *IEEE Trans. Veh. Technol.*, vol. 71, no. 6, pp. 6228–6244, Jun. 2022.
[64] P. Stoica, J. Li, and Y. Xie, "On probing signal design for MIMO radar," *IEEE Trans. Signal Process.*, vol. 55, no. 8, pp. 4151–4161, Aug. 2007.
[65] A. S. Bandeira, N. Boumal, and A. Singer, "Tightness of the maximum likelihood semidefinite relaxation for angular synchronization," *Math. Program.*, vol. 163, pp. 145–167, May 2017.
[66] S. H. Low, "Convex relaxation of optimal power flow—Part II: Exactness," *IEEE Trans. Control Netw. Syst.*, vol. 1, no. 2, pp. 177–189, Jun. 2014.
[67] C. Lu, Y.-F. Liu, W.-Q. Zhang, and S. Zhang, "Tightness of a new and enhanced semidefinite relaxation for MIMO detection," *SIAM J. Optim.*, vol. 29, no. 1, pp. 719–742, 2019.
[68] R. El-Sehiemy, M. A. Hamida, E. Elattar, A. Shaheen, and A. Ginidi, "Nonlinear dynamic model for parameter estimation of Li-ion batteries using supply–demand algorithm," *Energies*, vol. 15, no. 13, p. 4556, 2022.
[69] P. Li et al., "RIS-assisted high-speed railway integrated sensing and communication system," *IEEE Trans. Veh. Technol.*, vol. 72, no. 12, pp. 15681–15692, Dec. 2023.
[70] R. Liu, M. Li, H. Luo, Q. Liu, and A. L. Swindlehurst, "Integrated sensing and communication with reconfigurable intelligent surfaces: Opportunities, applications, and future directions," *IEEE Wireless Commun.*, vol. 30, no. 1, pp. 50–57, Feb. 2023.
[71] J. Liang et al., "Problem definitions and evaluation criteria for the CEC 2017 competition on constrained real-parameter optimization," in *Proc. IEEE Congr. Evol. Computation (CEC)*, 2017, pp. 2834–2841.
[72] J. B. Sanson, D. Castanheira, A. Gameiro, and P. P. Monteiro, "Cooperative method for distributed target tracking for OFDM radar with fusion of radar and communication information," *IEEE Sensors J.*, vol. 21, no. 14, pp. 15584–15597, Jul. 2021.
[73] K. Meng, Q. Wu, S. Ma, W. Chen, and T. Q. S. Quek, "UAV trajectory and beamforming optimization for integrated periodic sensing and communication," *IEEE Wireless Commun. Lett.*, vol. 11, no. 6, pp. 1211–1215, Jun. 2022.

MOHAMED I. ISMAIL received the B.S. degree in electronics and communications engineering from the Modern Academy for Engineering and Technology, Cairo, Egypt, in 2008, the M.S. degree in electronics and communications from Arab Academy for Science, Technology and Maritime Transport Cairo, Egypt, in 2014, and the Ph.D. degree from the Communications and Electronics Department, Suez Canal University, Ismailia, Egypt, in 2019. He is an Assistant Professor with the Modern Academy for Engineering and Technology, with expertise in signal processing, communication networks, MIMO systems, cooperative communications, and interference networks. He has made significant contributions to the field of engineering and international relations. He was a member of the Committee of International Relations and African Affairs at the Egyptian Engineering Syndicate from 2017 to 2022, where he contributed to the capacity-building program for international fresh graduate engineers. He was also a member of the strategic planning committee at the Federation of African Engineering Organization from 2020 to 2022. Additionally, he represented the ESE in Zambia to activate the protocol of the capacity-building program between the ESE and the Engineering institution of Zambia EIZ from 2019 to 2020.

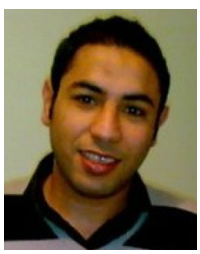

ABDULLAH M. SHAHEEN was born in Tanta, Egypt, in 1985. He received the B.Sc. degree from Suez Canal University, Port-Said, Egypt, in 2007, and the M.Sc. and Ph.D. degrees from Menoufia University, Shebin El-Kom, Egypt, in 2012 and 2016, respectively. He is currently with the Department of Electrical Engineering, Faculty of Engineering, Suez University, El-Suweis, Egypt. His research interests include power system operation, control, and planning, the applications of optimization algorithms in electric power systems, renewable integration, and smart grids.

MOSTAFA M. FOUDA (Senior Member, IEEE) received the B.S. and M.S. degrees in electrical engineering from Benha University, Egypt, in 2002 and 2007, respectively, and the Ph.D. degree in information sciences from Tohoku University, Japan, in 2011. He is currently an Associate Professor with the Department of Electrical and Computer Engineering, Idaho State University, ID, USA. He also holds the position of a Full Professor with Benha University. He was an Assistant Professor with Tohoku University and a Postdoctoral Research Associate with Tennessee Technological University, TN, USA. He has (co)authored more than 220 technical publications. His current research focuses on cybersecurity, communication networks, signal processing, wireless mobile communications, smart healthcare, smart grids, AI, and IoT. He has received several research grants, including NSF Japan-U.S. Network Opportunity 3. He has guest-edited a number of special issues covering various emerging topics in communications, networking, and health analytics. He is currently serving on the editorial board of IEEE TRANSACTIONS ON VEHICULAR TECHNOLOGY, IEEE INTERNET OF THINGS JOURNAL, and IEEE ACCESS.

AHMED S. ALWAKEEL received the B.S. degree in electronics and communications engineering from Cairo University, Giza, Egypt, in 2006, and the M.S. degree in electronics and communications from Port Said University, Port Fuad, Egypt, in 2014, and the Ph.D. degree from the Communications and Electronics Department, Suez Canal University, Ismailia, Egypt, in 2018. He is currently an Assistant Professor with Suez University. His current research interests include large-scale (massive) MIMO systems, cooperative communications, and interference networks.